The Astrophysical Journal, 428:574–590, 1994 June 20

LYMAN-ALPHA ABSORPTION IN THE SPECTRUM OF THE $z = 4.5$ QSO BR 1033−0327

G. M. Williger,[1,2] J. A. Baldwin,[1] R. F. Carswell,[3,4] A. J. Cooke,[3] C. Hazard,[3,5]
M. J. Irwin,[6] R. G. McMahon,[3] and L. J. Storrie-Lombardi[3]

Received 1993 August 9; accepted 1993 December 16

ABSTRACT

We present the results of echelle spectroscopy of the Lyα forest region in the spectrum of the bright ($m_R = 18.5$) optically selected $z = 4.5$ QSO BR 1033−0327. These results, which extend Lyα forest absorption line studies up to a redshift of $z = 4.5$ at a resolution of 12 km s^{-1}, represent the first high-resolution study of Lyα forest systems at such high redshifts.

We compare the properties of the Lyα forest systems in the redshift range $3.7 < z < 4.3$ with those inferred from similar observations at $1.86 < z < 3.27$ and find some clear indications of redshift dependence in these. First, the ionizing flux from the quasar appears to affect the Lyα line density further from the QSO than at lower redshifts, implying that the Lyman limit background flux at redshift $z \sim 4.2$ is $J_\nu \sim 1\text{–}3 \times 10^{-22}$ ergs cm^{-2} s^{-1} Hz^{-1} sr^{-1}. This is about a factor of 10 lower than estimates at $z \sim 2.5$. Second, the Doppler parameter distribution for systems where the effect of the QSO ionizing flux is small ($3.7 < z < 4.3$) has an excess at values ~ 20 km s^{-1}, compared with lower redshifts; we suggest this may be due to the lower ionizing flux at $z \sim 4.2$, which would reduce the heating of the gas. Finally, while there is no evidence that the shape of the H I column density distribution changes significantly, the redshift dependence of the total number of systems is stronger than that found at lower redshifts, with the number of systems per unit redshift $\sim (1 + z)^{4.6}$. Also, over the entire redshift range there is no significant correlation between Doppler parameter and H I column density and no signal in the two-point correlation function down to velocity separations of $\Delta v \sim 100$ km s^{-1}. There is no evidence for continuously distributed H I absorption (the Gunn-Peterson effect) at these redshifts.

Subject headings: intergalactic medium — quasars: absorption lines — quasars: individual (BR 1033−0327)

1. INTRODUCTION

The population of sharp absorption features shortward of Lyα emission in high-redshift QSOs, known as the Lyα forest, has received much observational and theoretical attention in the past decade. These systems have the potential to yield important information on the intergalactic medium and galaxy formation and on the background ionizing flux at high redshifts. Despite the effort put into understanding the nature and origin of the objects giving rise to the Lyα forest (reviewed by Bechtold 1987; more recently by Wolfe 1991), they remain enigmatic.

There is, however, a wealth of detailed information which provides some indications of their general properties. The number density of these systems rises rapidly with increasing redshift (Lu, Wolfe, & Turnshek 1991), they show little sign of clustering on scales one might expect if they arise in galaxies (Sargent et al. 1980), and the heavy-element abundances are generally believed to be low (Chaffee et al. 1986). These points in particular have led to the suggestion that the Lyα forest systems are intergalactic and the material in them has undergone little nuclear processing in stars.

The most detailed information about Lyα clouds comes from high signal-to-noise, high-resolution ($R \geq 10^4$ to resolve the majority of the lines) spectra. Fitting line profiles to the absorption features allows the determination of H I column density $N_{\rm H\,I}$ and Doppler parameter b for each component in an absorption line complex. The distribution functions of cloud numbers with respect to these quantities as a function of redshift provide links between observations and the predictions of different general classes of models, such as those for gravitationally confined clouds (Bond, Szalay, & Silk 1988; Murakami & Ikeuchi 1993; Miralda-Escudé & Rees 1993) and for pressure-confined clouds (Ikeuchi & Ostriker 1986; Williger & Babul 1992). High-resolution spectra provide information up to $z \sim 0.16$ from *Hubble Space Telescope* (*HST*) observations (Morris et al. 1991), and from $z \sim 1.8$ (Carswell et al. 1991a) to $z \sim 3.8$ (Carswell et al. 1987) using ground-based telescopes. These studies have shown that, apart from the number density of Lyα systems, there has been little change in the distributions of the parameters over the redshift range $1.8 < z < 3.8$, and possibly down to zero redshift. Observational results which have the potential to constrain the models strongly, such as correlations between Doppler parameter and H I column density (Pettini et al. 1990), may well arise predominantly from selection effects (Rauch et al. 1993). Other clues as to the nature of the absorbers, such as (1) any feature in the H I column density distribution which would serve to identify clouds at different redshifts as arising from similar systems, or (2) evidence for temperature changes, have remained elusive.

Here we extend the redshift baseline for such observations out to $z \sim 4.5$ and probe the conditions in the clouds at early

---

[1] Cerro Tololo Inter-American Observatory, Casilla 603, La Serena, Chile. Operated by the Association of Universities for Research in Astronomy (AURA), Inc., under cooperative agreement with the National Science Foundation.

[2] Present address: Max-Planck-Institut für Astronomie, Königstuhl 17, D-69117 Heidelberg, Germany.

[3] Institute of Astronomy, Madingley Road, Cambridge CB3 0HA, England.

[4] Visiting Astronomer, Cerro Tololo Inter-American Observatory.

[5] Postal address: Department of Physics and Astronomy, University of Pittsburgh, 100 Allen Hall, Pittsburgh, PA 15260.

[6] Royal Greenwich Observatory, Madingley Road, Cambridge CB3 0EZ, England.

epochs through the distribution functions of their line parameters. The background QSO in this case is BR 1033−0327, $z = 4.506$, $m_R = 18.5$, $R-I \sim 0$, which was discovered by Irwin, McMahon, & Hazard (1991, 1994) as part of a program to search for the highest redshift QSOs. The coordinates of this object are $\alpha = 10^{h}33^{m}51^{s}.5$, $\delta = -3°27'46''$ (1950.0). Results from a low-resolution study of the Lyman limit absorption systems in $z > 4.2$ QSOs discovered in the same program are described by Storrie-Lombardi et al. (1994).

2. OBSERVATIONS AND REDUCTIONS

Our observations were made on 1992 February 27 and 28 at the Cerro Tololo Inter-American Observatory (CTIO) 4 m telescope in conditions of 1″.5 seeing and good transparency. We used the Cassegrain echelle spectrograph with its long-focal-length camera and a thinned Tek2048^2 CCD. The slit width was 1″.25. The wavelength coverage was 4483–8092 Å with spectral overlap to 5664 Å. The slit length was 13″, which ensured an adequate sky signal for sky subtraction with no spatial overlap between adjacent spectral orders. The total exposure time was 55,000 s, broken into eight individual exposures of ∼2 hr. Basic bias subtraction and flat-fielding were done with standard IRAF packages. The spectra then were extracted optimally using similar programs to those used by Rauch et al. (1992), which also produce error estimates based on photon statistics. A signal-to-noise ratio of 10–15 per

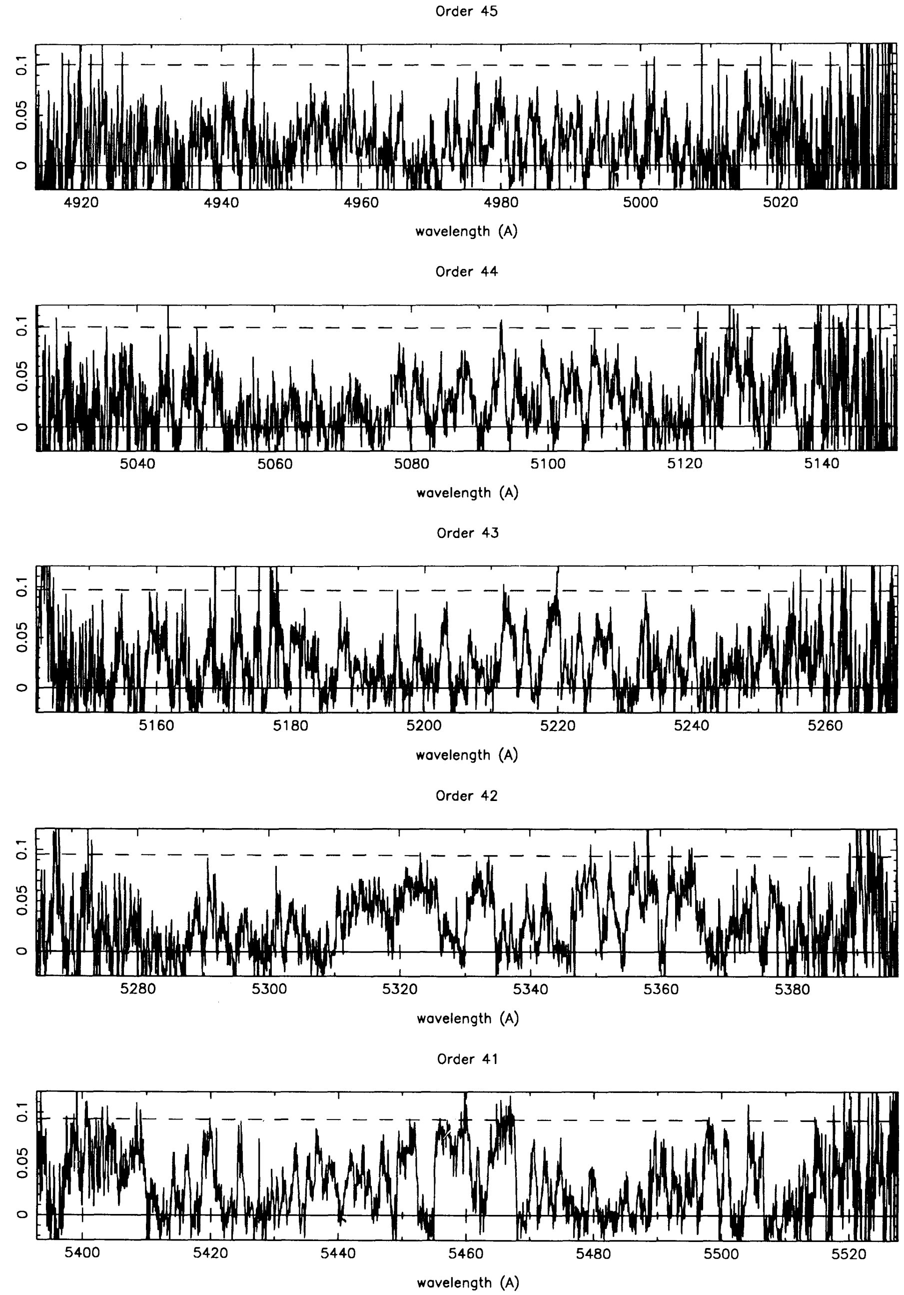

FIG. 1.—Echelle spectrum of BR 1033−0327. The flux scale is approximate and in units of 10^{-15} ergs cm^{-2} s^{-1} Hz^{-1}. The dashed line shows the continuum in the region shortward of the Lyα emission line, and tick marks indicate the positions of the fitted Lyα absorption lines. Single channels with zero intensity are noise spikes, which were zero weighted in the analysis.

resolution element was obtained in the continuum between Lyα and Lyβ emission, where the monochromatic continuum magnitude is $m \approx 18$. Thorium-argon comparison lamp frames taken before and after each object exposure were extracted and summed to determine the wavelength scale.

Summed, sky-subtracted spectra were constructed by rebinning each individual frame to the same heliocentric linear wavelength scale for each echelle order and adding them, weighting by the inverse of the variance. Bad columns and cosmic rays were zero weighted. The resultant spectrum is shown in Figure 1.

The comparison lamp spectra for each frame were linearized and summed using the same weights as the corresponding object integration, and this sum was used to determine the spectral resolution. Low-order polynomials were fitted to the comparison line widths in each order, and these were used to determine the instrument profile in the subsequent analysis. The resolution is typically 12 km s^{-1} full width at half-maximum.

Low-resolution (~ 5 Å) observations were obtained with the William Herschel Telescope (WHT) on La Palma on 1993 April 17, using the two-beam ISIS spectrograph with 158 line mm^{-1} gratings. In the red arm, we used an English Electric Valve (EEV) detector with 22.5 μm pixels and covered the wavelength range 5700–8800 Å. In the blue arm, we used a thinned Tek1024^2 detector with 24 μm pixels and covered the

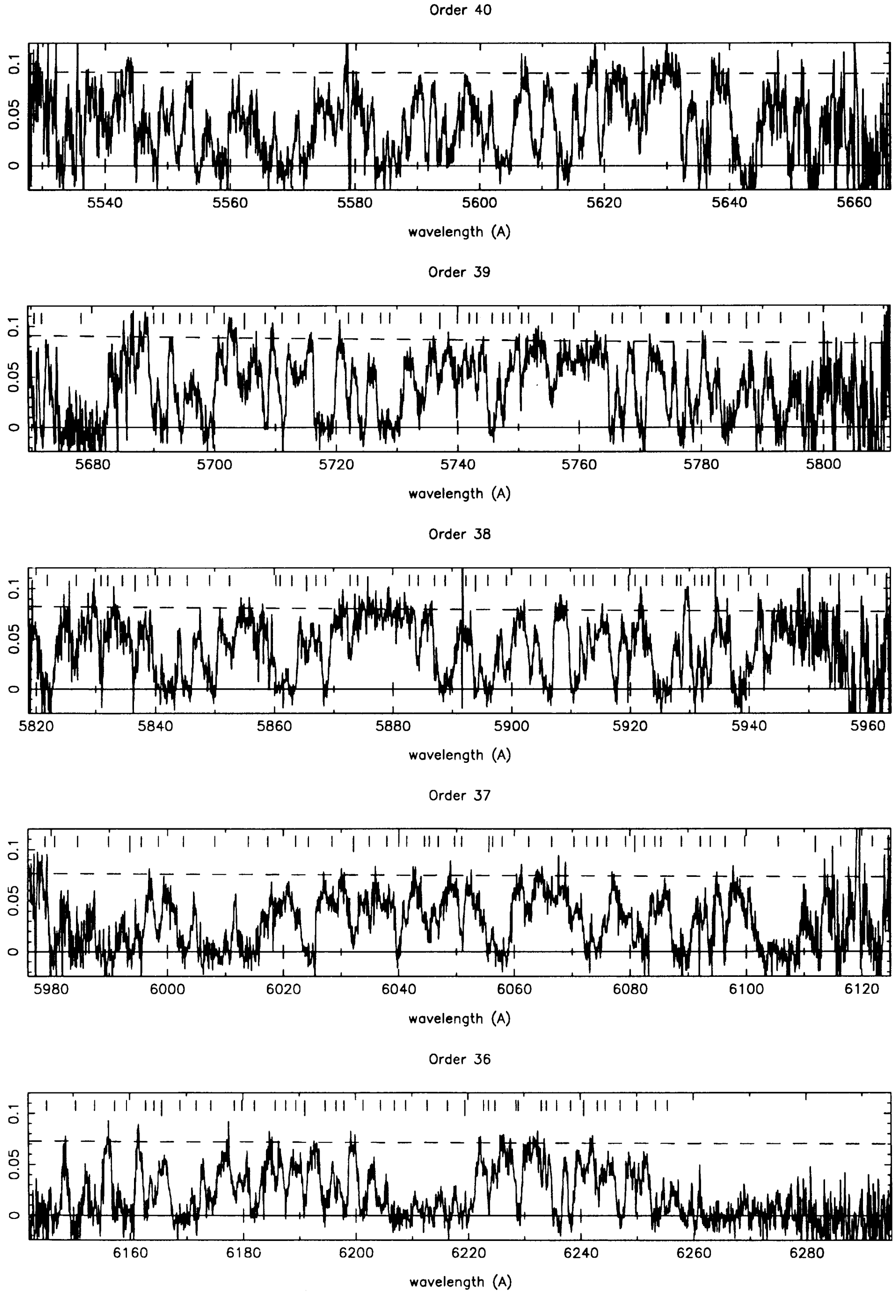

FIG. 1—*Continued*

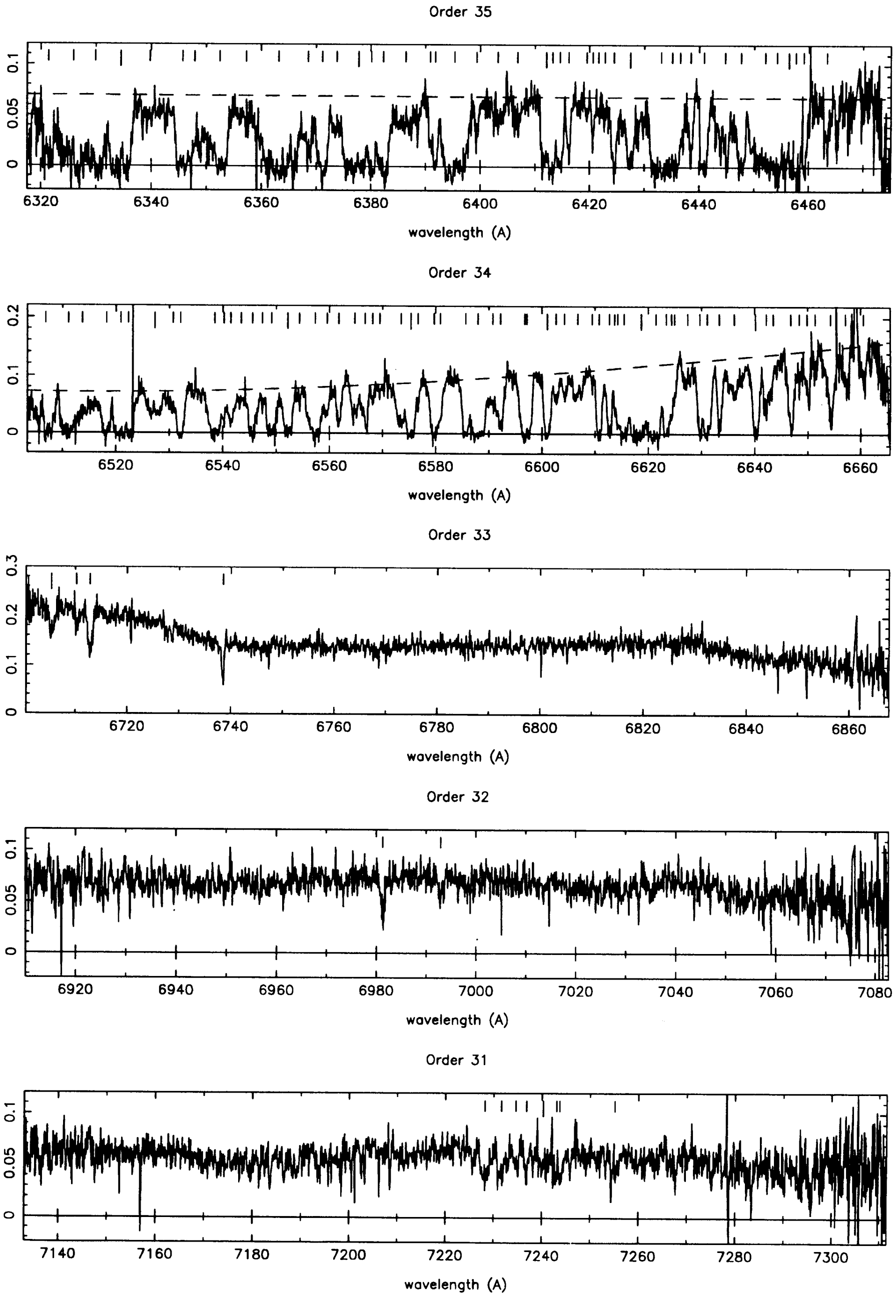

FIG. 1—*Continued*

wavelength range 3300–6000 Å. Three 900 s exposures in the red and two 1500 s exposures in the blue were obtained. These were bias subtracted, flat-fielded, extracted, and flux-calibrated using IRAF packages. The spectrum is shown in Figure 2.

A continuum for the echelle data was constructed by extrapolating a power-law fit to the flux redward of Lyα emission from the low-dispersion spectrum, renormalized so that the fluxes integrated over the width of an echelle order in the echelle data and the low-resolution data matched. This continuum passes through the (few) regions of highest flux in the Lyα forest, which provides independent evidence that our continuum estimate is a good one.

Voigt profiles were convolved with a Gaussian having the same full width at half-maximum as the instrumental resolution at that wavelength and then fitted to the observed profiles (see Rauch et al. 1993, and references therein, for details). The data have incomplete wavelength coverage at longer wavelengths and do not extend out to C IV emission, so the identification of heavy-element absorption systems is difficult. Therefore, all absorption features between Lyα and Lyβ emission are assumed to be Lyα lines. This will result in some contamination of the Lyα sample, but the Lyα line density is so much higher than the expected heavy-element line density that such contamination will not be important. We fitted all absorption complexes between the QSO Lyα and Lyβ emission save for interorder gaps, so there is (incomplete) coverage over the redshift range $3.66 < z < 4.47$. The results are contained in Table 1. Higher order Lyman lines were fitted simultaneously

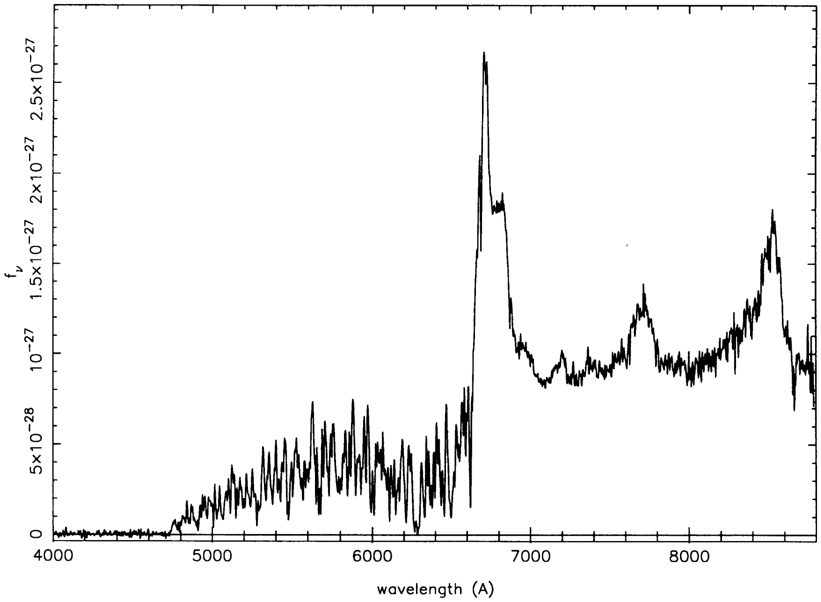

FIG. 2.—Low-resolution spectrum of BR 1033−0327. The flux scale is in ergs cm^{-2} s^{-1} Hz^{-1}.

wherever they provided constraints on the Doppler parameter and H I column density. Those which provide useful constraints are shown for each Lyα line in Table 1. We do not give the parameters for the additional Lyα systems for redshifts $z < 3.66$, since these are based only on Lyα in all cases and they are additionally affected by any uncertainties in the higher-order Lyman lines from higher redshift systems with which they are blended. A sample spectral region showing the data and the fitted Lyα profiles (convolved with the instrument profile) is shown in Figure 3.

3. HEAVY-ELEMENT SYSTEMS

We are able to identify C IV absorption systems at $z = 3.51$ and $z \sim 3.67$ and a damped Lyα absorption system at $z = 4.16$, each containing some lines longward of the Lyα forest region of the spectrum. Possibly, corresponding heavy elements in the Lyα forest were lost in Lyα absorption complexes.

3.1. *The* $z = 3.51$ *System*

This is identified by a single C IV doublet just longward of 6980 Å at $z = 3.509283 \pm 0.000027$, $b = 21.3 \pm 2.6$, and $\log N = 13.51 \pm 0.04$. The corresponding Lyα is at 5482 Å and is subject to confusion from Lyβ absorption at redshifts $z \sim 4.345$. The Lyα corresponding to any confusing Lyβ falls at 6497 Å and so is not covered in the echelle spectrum.

3.2. *The* $z = 3.67$ *Complex*

A complex of C IV lines extending over 7225–7255 Å provides the basis for this group (see Table 1). The corresponding Lyα lines are just longward of the Lyβ emission line at 5678.2 Å

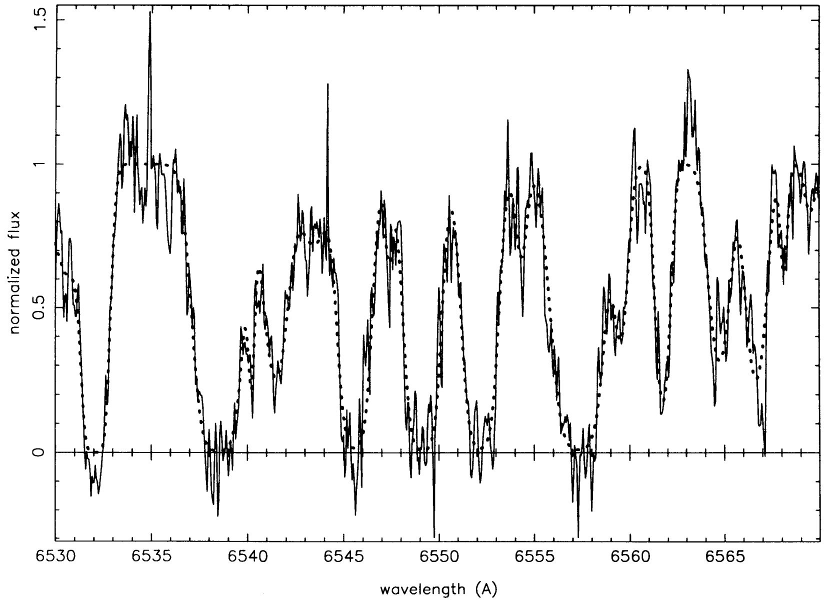

FIG. 3.—Region of the spectrum of BR 1033−0327 showing the data normalized to unit continuum (*continuous line*) and the Voigt profile fits convolved with the instrument profile (*dotted line*).

TABLE 1

BR 1033−0327 ABSORPTION LINE PARAMETERS

n	λ_{vac}	ID	z	±	b	±	$\log N$	±	w_λ	p	Comments
1	5670.52	Lyα	3.66453	0.00006	11	18	14.47	4.22	0.16	0.03	α
2	5671.73	Lyα	3.66552	0.00006	12	16	14.50	3.15	0.18		α
3	5678.22	Lyα	3.67086	0.00007	62	2	19.14	0.05	2.99		α
4	5690.12	Lyα	3.68065	0.00003	25	3	14.01	0.08	0.24	0.53	α
5	5691.68	Lyα	3.68193	0.00003	18	4	15.28	0.87	0.32		α
6	5694.40	Lyα	3.68417	0.00009	38	6	14.15	0.13	0.36		α
7	5696.28	Lyα	3.68572	0.00025	72	60	13.91	0.34	0.34		α
8	5698.82	Lyα	3.68781	0.00010	53	5	14.53	0.09	0.60		α
9	5701.66	Lyα	3.69014	0.00006	20	5	13.15	0.09	0.06		α
10	5704.98	Lyα	3.69287	0.00006	59	6	13.81	0.04	0.27	0.01	α
11	5708.33	Lyα	3.69563	0.00003	29	2	13.99	0.06	0.26		α
12	5711.13	Lyα	3.69793	0.00003	32	2	14.02	0.04	0.28	0.52	α
13	5713.84	Lyα	3.70016	0.00007	70	7	13.77	0.04	0.26		α
14	5718.12	Lyα	3.70368	0.00002	40	3	15.95	0.29	0.76	0.90	$\alpha\beta$
15	5722.06	Lyα	3.70693	0.00003	19	3	13.74	0.07	0.16	0.01	α
16	5724.25	Lyα	3.70872	0.00003	24	3	14.57	0.22	0.33		$\alpha\beta$
17	5727.32	Lyα	3.71125	0.00041	266	34	14.24	0.06	0.81		$\alpha\beta$
18	5728.84	Lyα	3.71250	0.00003	52	5	15.65	0.32	0.90		$\alpha\beta$
19	5733.95	Lyα	3.71670	0.00004	52	4	13.97	0.04	0.33		α
20	5737.06	Lyα	3.71926	0.00005	36	4	13.48	0.05	0.13		α
21	5739.98	Lyα	3.72167	0.00006	52	6	13.66	0.04	0.20		α
22	5741.91	Lyα	3.72326	0.00006	22	6	13.18	0.09	0.07		α
23	5743.17	Lyα	3.72429	0.00004	22	3	13.40	0.05	0.10		α
24	5745.71	Lyα	3.72638	0.00003	36	3	14.34	0.08	0.40		α
25	5747.49	Lyα	3.72784	0.00003	20	3	13.77	0.08	0.17		α
26	5748.60	Lyα	3.72876	0.00022	44	18	13.38	0.17	0.11		α
27	5750.57	Lyα	3.73038	0.00004	16	5	13.21	0.16	0.07		α
28	5751.69	Lyα	3.73130	0.00046	61	39	13.12	0.26	0.07		α
29	5755.59	Lyα	3.73450	0.00004	34	4	13.62	0.05	0.17	0.22	α
30	5759.14	Lyα	3.73742	0.00040	290	39	13.95	0.05	0.45		α
31	5765.45	Lyα	3.74262	0.00002	18	2	14.67	0.21	0.27		$\alpha\beta$
32	5767.08	Lyα	3.74396	0.00002	26	3	14.09	0.08	0.27		α
33	5770.16	Lyα	3.74649	0.00002	32	3	14.57	0.15	0.42		α
34	5774.32	Lyα	3.74991	0.00027	107	23	13.77	0.10	0.28		α
35	5774.69	Lyα	3.75022	0.00003	20	4	13.85	0.10	0.19		α
36	5776.72	Lyα	3.75189	0.00002	17	3	15.32	0.58	0.31		$\alpha\beta$
37	5778.87	Lyα	3.75365	0.00003	40	3	14.17	0.05	0.38		α
38	5781.63	Lyα	3.75593	0.00006	34	5	13.75	0.07	0.21	0.11	α
39	5784.57	Lyα	3.75835	0.00005	64	7	14.60	0.08	0.72		α
40	5787.41	Lyα	3.76068	0.00006	27	6	13.53	0.08	0.14		α
41	5789.39	Lyα	3.76231	0.00003	31	4	14.32	0.15	0.36		α
42	5793.01	Lyα	3.76529	0.00008	70	7	14.47	0.07	0.69		α
43	5797.64	Lyα	3.76909	0.00013	92	13	14.48	0.07	0.82		α
44	5806.37	Lyα	3.77628	0.00033	216	38	14.76	0.06	1.74		α
	5809– 5819 not covered										
45	5821.90	Lyα	3.78905	0.00006	72	5	14.49	0.06	0.72	1.00	α
46	5826.77	Lyα	3.79306	0.00012	83	12	13.90	0.05	0.34	0.70	α
47	5830.92	Lyα	3.79647	0.00004	19	4	13.72	0.09	0.16	0.35	α
48	5832.07	Lyα	3.79741	0.00015	29	14	13.20	0.16	0.08		α
49	5834.51	Lyα	3.79942	0.00016	39	13	13.35	0.14	0.10	0.08	α
50	5836.62	Lyα	3.80116	0.00009	54	8	13.86	0.05	0.29		α
51	5838.81	Lyα	3.80296	0.00003	8	4	13.19	0.13	0.05		α
52	5840.38	Lyα	3.80425	0.00006	33	5	14.23	0.09	0.35		α
53	5842.48	Lyα	3.80598	0.00004	26	5	15.99	0.70	0.52		$\alpha\beta$
54	5845.39	Lyα	3.80837	0.00003	49	4	14.34	0.05	0.49		α
55	5849.14	Lyα	3.81146	0.00003	46	3	14.56	0.08	0.55		$\alpha\beta$
56	5852.50	Lyα	3.81422	0.00006	58	6	13.79	0.04	0.26		α
57	5860.27	Lyα	3.82061	0.00074	184	33	14.16	0.14	0.65	0.18	α
58	5861.01	Lyα	3.82122	0.00006	32	4	14.63	0.11	0.43		$\alpha\beta$
59	5863.00	Lyα	3.82286	0.00005	26	4	14.62	0.15	0.37		$\alpha\beta$
60	5865.44	Lyα	3.82487	0.00007	38	9	13.60	0.14	0.17		α
61	5867.03	Lyα	3.82617	0.00005	18	5	13.27	0.09	0.08		α
62	5868.63	Lyα	3.82749	0.00003	33	3	14.18	0.06	0.34		α

1994ApJ...428..574W

TABLE 1—*Continued*

n	$\lambda_{\rm vac}$	ID	z	±	b	±	$\log N$	±	w_λ	p	Comments
63	5872.81	Lyα	3.83093	0.00004	22	3	13.44	0.05	0.11	0.02	α
64	5874.06	Lyα	3.83196	0.00003	4	6	12.78	0.33	0.02		α
65	5882.80	Lyα	3.83914	0.00003	2	9	12.92	2.75	0.02		α
66	5884.27	Lyα	3.84035	0.00003	22	2	13.54	0.04	0.13		α
67	5887.02	Lyα	3.84262	0.00003	3	10	14.72	11.69	0.06	0.30	α
68	5888.82	Lyα	3.84410	0.00005	57	6	14.59	0.08	0.66		α
69	5892.35	Lyα	3.84701	0.00050	113	92	13.78	0.32	0.29		α
70	5893.96	Lyα	3.84833	0.00002	13	2	14.79	0.31	0.21		$\alpha\beta$
71	5896.04	Lyα	3.85004	0.00005	50	6	14.52	0.09	0.57		α
72	5899.17	Lyα	3.85262	0.00004	49	3	13.97	0.03	0.33		α
73	5903.22	Lyα	3.85594	0.00003	34	2	13.78	0.03	0.22		α
74	5905.84	Lyα	3.85810	0.00002	33	2	14.97	0.11	0.50		$\alpha\beta$
75	5910.61	Lyα	3.86202	0.00002	27	3	14.66	0.20	0.38	0.83	α
76	5912.31	Lyα	3.86342	0.00003	17	2	13.64	0.06	0.13		α
77	5913.79	Lyα	3.86464	0.00007	39	7	13.55	0.07	0.15		α
78	5917.45	Lyα	3.86765	0.00003	21	4	14.18	0.22	0.25		α
79	5917.49	Lyα	3.86768	0.00021	105	40	13.77	0.06	0.27		α
80	5919.80	Lyα	3.86958	0.00003	18	3	13.58	0.07	0.13		α
81	5920.89	Lyα	3.87048	0.00005	19	6	13.08	0.12	0.06		α
82	5922.79	Lyα	3.87205	0.00010	28	9	13.25	0.12	0.08	0.10	α
83	5925.47	Lyα	3.87425	0.00004	56	3	14.96	0.08	0.78		$\alpha\beta$
84	5927.92	Lyα	3.87627	0.00005	10	6	13.03	0.13	0.05		α
85	5928.59	Lyα	3.87682	0.00002	8	3	14.05	0.48	0.11		$\alpha\beta$
86	5930.90	Lyα	3.87872	0.00004	24	4	14.15	0.14	0.27	0.02	α
87	5932.11	Lyα	3.87971	0.00003	12	4	13.89	0.32	0.13		α
88	5933.25	Lyα	3.88065	0.00004	26	4	13.90	0.07	0.22		α
89	5935.80	Lyα	3.88275	0.00008	34	7	13.34	0.07	0.10	0.20	α
90	5938.23	Lyα	3.88474	0.00004	26	1	16.30	0.17	0.56		α
91	5940.32	Lyα	3.88646	0.00010	39	7	13.86	0.07	0.26		$\alpha\beta$
92	5943.07	Lyα	3.88872	0.00005	36	4	13.76	0.05	0.21	0.46	α
93	5953.72	Lyα	3.89748	0.00338	395	196	14.36	0.30	1.08	0.70	α
94	5957.66	Lyα	3.90073	0.00010	15	3	17.94	0.41	0.74		$\alpha\beta$
95	5961.25	Lyα	3.90368	0.00010	48	7	14.85	0.11	0.66		$\alpha\beta$
	5963– 5977 not covered										
96	5978.94	Lyα	3.91823	0.00008	8	9	12.89	0.24	0.03	0.31	α
97	5980.55	Lyα	3.91956	0.00004	27	3	14.98	0.25	0.42		$\alpha\beta$
98	5984.55	Lyα	3.92285	0.00012	96	12	14.53	0.05	0.89		α
99	5989.84	Lyα	3.92720	0.00009	83	15	14.86	0.16	1.03		α
100	5993.55	Lyα	3.93025	0.00006	32	9	14.42	0.25	0.39		α
101	5995.47	Lyα	3.93183	0.00009	40	6	14.05	0.06	0.33		α
102	5998.41	Lyα	3.93425	0.00005	44	4	13.88	0.04	0.28	0.32	α
103	6002.76	Lyα	3.93783	0.00005	73	4	14.41	0.03	0.67		α
104	6008.17	Lyα	3.94228	0.00003	54	7	17.37	0.81	1.32		$\alpha\beta$
105	6013.98	Lyα	3.94706	0.00004	50	4	15.47	0.17	0.85		$\alpha\beta$
106	6017.31	Lyα	3.94979	0.00069	178	49	14.23	0.13	0.73		α
107	6022.12	Lyα	3.95375	0.00009	28	8	13.41	0.13	0.11		α
108	6024.34	Lyα	3.95558	0.00005	48	5	14.64	0.13	0.60		α
109	6028.42	Lyα	3.95893	0.00012	88	14	13.71	0.05	0.24		α
110	6032.15	Lyα	3.96200	0.00005	51	4	14.02	0.03	0.36	0.10	α
111	6034.85	Lyα	3.96422	0.00010	49	10	13.63	0.09	0.19		α
112	6037.94	Lyα	3.96676	0.00016	87	26	13.78	0.09	0.28		α
113	6039.98	Lyα	3.96844	0.00002	18	2	14.34	0.10	0.24		$\alpha\beta$
114	6041.36	Lyα	3.96958	0.00005	30	5	13.57	0.05	0.15		α
115	6044.41	Lyα	3.97208	0.00038	54	18	13.67	0.21	0.21		α
116	6045.24	Lyα	3.97277	0.00005	16	7	13.41	0.23	0.10		α
117	6046.80	Lyα	3.97406	0.00017	64	11	13.84	0.08	0.29		α
118	6049.64	Lyα	3.97639	0.00012	21	11	12.81	0.17	0.03		α
119	6050.87	Lyα	3.97740	0.00003	21	2	13.72	0.05	0.16		α
120	6055.62	Lyα	3.98131	0.00004	14	3	14.13	0.18	0.18		$\alpha\beta$
121	6056.23	Lyα	3.98181	0.00013	152	10	14.34	0.05	0.84		$\alpha\beta$
122	6057.91	Lyα	3.98319	0.00003	36	2	15.26	0.11	0.60		$\alpha\beta\gamma$
123	6062.48	Lyα	3.98695	0.00005	41	4	13.58	0.04	0.16		α

TABLE 1—*Continued*

n	$\lambda_{\rm vac}$	ID	z	±	b	±	log N	±	w_λ	p	Comments
124	6066.47	Lyα	3.99024	0.00012	69	11	13.49	0.05	0.15	0.59	α
125	6070.32	Lyα	3.99340	0.00007	64	8	13.84	0.04	0.29		α
126	6072.53	Lyα	3.99522	0.00002	22	2	14.56	0.09	0.31		$\alpha\beta$
127	6074.37	Lyα	3.99673	0.00003	26	2	14.74	0.09	0.38		$\alpha\beta\gamma$
128	6075.93	Lyα	3.99801	0.00005	25	4	13.60	0.06	0.15		α
129	6079.25	Lyα	4.00074	0.00015	73	11	13.91	0.06	0.33		α
130	6080.82	Lyα	4.00204	0.00004	18	4	13.87	0.10	0.18		$\alpha\beta$
131	6082.48	Lyα	4.00340	0.00004	37	4	14.24	0.07	0.38		$\alpha\beta$
132	6084.31	Lyα	4.00490	0.00005	15	6	13.18	0.22	0.06		α
133	6085.34	Lyα	4.00575	0.00020	45	19	13.42	0.16	0.12		α
134	6088.89	Lyα	4.00867	0.00004	50	5	15.29	0.21	0.79		$\alpha\beta$
135	6092.16	Lyα	4.01137	0.00010	55	13	13.81	0.07	0.26		$\alpha\beta$
136	6093.83	Lyα	4.01274	0.00002	14	2	14.28	0.25	0.20		$\alpha\beta$
137	6096.41	Lyα	4.01486	0.00003	33	2	13.89	0.04	0.25		$\alpha\beta$
138	6099.76	Lyα	4.01762	0.00009	42	8	13.53	0.07	0.15	1.00	α
139	6105.50	Lyα	4.02234	0.00006	104	7	15.80	0.17	1.75		$\alpha\beta$
140	6111.93	Lyα	4.02763	0.00007	52	6	14.32	0.09	0.50		α
141	6116.33	Lyα	4.03125	0.00007	45	4	14.50	0.06	0.52		$\alpha\beta$
142	6121.87	Lyα	4.03581	0.00034	143	31	14.50	0.08	1.03		α
	6124– 6143 not covered										
143	6145.27	Lyα	4.05505	0.00005	54	5	16.25	0.34	1.07	0.77	$\alpha\beta$
144	6150.39	Lyα	4.05927	0.00004	44	4	14.84	0.14	0.61		$\alpha\beta\gamma$
145	6153.78	Lyα	4.06205	0.00005	45	5	14.64	0.16	0.57		$\alpha\gamma$
146	6157.32	Lyα	4.06497	0.00004	22	3	14.02	0.12	0.23	0.90	α
147	6159.44	Lyα	4.06671	0.00003	35	2	15.26	0.12	0.58		$\alpha\beta\gamma\delta$
148	6162.81	Lyα	4.06948	0.00003	23	3	14.02	0.08	0.24	0.91	α
149	6164.29	Lyα	4.07070	0.00006	26	6	13.80	0.09	0.20		α
150	6165.63	Lyα	4.07180	0.00023	37	22	13.33	0.24	0.10		α
151	6168.84	Lyα	4.07444	0.00003	44	2	15.87	0.14	0.83		$\alpha\beta\gamma\delta$
152	6171.72	Lyα	4.07681	0.00003	20	2	14.50	0.07	0.27		$\alpha\beta$
153	6174.31	Lyα	4.07894	0.00005	69	4	14.16	0.03	0.49		α
154	6178.50	Lyα	4.08238	0.00005	33	4	13.77	0.05	0.21	0.36	α
155	6179.82	Lyα	4.08348	0.00007	20	7	13.32	0.14	0.09		α
156	6182.07	Lyα	4.08532	0.00007	71	6	14.24	0.03	0.55		$\alpha\beta$
157	6185.74	Lyα	4.08835	0.00004	25	4	13.46	0.05	0.12	0.49	α
158	6187.60	Lyα	4.08987	0.00003	28	3	13.75	0.04	0.19		$\alpha\beta$
159	6189.36	Lyα	4.09132	0.00010	36	12	13.35	0.11	0.10		α
160	6190.95	Lyα	4.09262	0.00004	27	3	13.78	0.05	0.20		α
161	6194.59	Lyα	4.09562	0.00003	38	3	14.15	0.04	0.36	0.42	α
162	6196.53	Lyα	4.09722	0.00004	23	4	13.58	0.06	0.14		α
163	6197.94	Lyα	4.09838	0.00003	25	3	14.14	0.08	0.27		α
164	6201.31	Lyα	4.10116	0.00003	37	2	14.23	0.05	0.38	0.46	$\alpha\beta$
165	6204.47	Lyα	4.10375	0.00014	57	9	14.14	0.07	0.43		$\alpha\beta$
166	6206.89	Lyα	4.10574	0.00023	43	14	14.46	0.17	0.49		$\alpha\beta$
167	6208.90	Lyα	4.10739	0.00008	38	5	15.07	0.10	0.59		$\alpha\beta$
168	6212.72	Lyα	4.11053	0.00008	90	12	14.73	0.05	1.00		$\alpha\beta$
169	6216.38	Lyα	4.11355	0.00004	30	3	14.69	0.15	0.42		$\alpha\beta$
170	6219.47	Lyα	4.11609	0.00003	52	2	14.95	0.06	0.73		$\alpha\beta$
171	6222.80	Lyα	4.11883	0.00014	25	10	13.15	0.16	0.07		α
172	6223.70	Lyα	4.11957	0.00004	15	3	13.63	0.08	0.12		α
173	6224.85	Lyα	4.12051	0.00007	31	7	13.40	0.07	0.11		α
174	6228.58	Lyα	4.12359	0.00016	93	17	13.60	0.06	0.20		$\alpha\beta$
175	6228.99	Lyα	4.12392	0.00002	16	2	14.40	0.15	0.22		$\alpha\beta$
176	6233.10	Lyα	4.12730	0.00002	10	2	13.20	0.06	0.06	0.74	α
177	6233.99	Lyα	4.12803	0.00002	9	2	13.19	0.07	0.06		α
178	6235.80	Lyα	4.12952	0.00002	28	1	14.84	0.08	0.42		$\alpha\beta\gamma$
179	6238.26	Lyα	4.13155	0.00003	26	2	14.16	0.10	0.28		α
180	6240.59	Lyα	4.13346	0.00006	40	5	13.49	0.04	0.14		α
181	6243.04	Lyα	4.13548	0.00005	22	6	13.42	0.15	0.11	0.62	$\alpha\beta$
182	6244.40	Lyα	4.13659	0.00024	76	19	13.71	0.11	0.23		α
183	6247.05	Lyα	4.13878	0.00003	30	3	14.39	0.13	0.37		α
184	6250.01	Lyα	4.14121	0.00007	66	7	13.86	0.04	0.30		α
185	6253.31	Lyα	4.14393	0.00004	34	3	14.65	0.11	0.46		$\alpha\beta$
186	6255.40	Lyα	4.14564	0.00004	29	4	14.10	0.06	0.29		α
	6257– 6318 not covered										

TABLE 1—*Continued*

n	$\lambda_{\rm vac}$	ID	z	±	b	±	$\log N$	±	w_λ	p	Comments
187	6321.39	Lyα	4.19993	0.00012	79	10	14.22	0.05	0.56	0.34	$\alpha\beta$
188	6325.96	Lyα	4.20368	0.00004	58	3	15.65	0.06	1.00		$\alpha\beta\gamma\delta$
189	6329.94	Lyα	4.20696	0.00005	58	3	15.05	0.04	0.83		$\alpha\beta$
190	6334.54	Lyα	4.21074	0.00002	39	3	16.53	0.29	0.84		$\alpha\beta\zeta$
191	6339.82	Lyα	4.21509	0.00030	143	37	13.83	0.09	0.32	0.31	α
192	6345.77	Lyα	4.21998	0.00004	36	4	14.84	0.16	0.52		$\alpha\beta$
193	6347.91	Lyα	4.22174	0.00029	146	20	14.38	0.05	0.88		$\alpha\beta$
194	6352.48	Lyα	4.22551	0.00006	61	5	14.47	0.05	0.64		$\alpha\beta$
195	6357.29	Lyα	4.22946	0.00026	114	27	13.78	0.08	0.29	0.06	α
196	6363.21	Lyα	4.23433	0.00003	81	2	15.90	0.05	1.45		$\alpha\beta\gamma$
197	6368.58	Lyα	4.23874	0.00005	48	5	13.97	0.04	0.33		$\alpha\beta\gamma$
198	6371.16	Lyα	4.24086	0.00002	24	1	15.47	0.08	0.44		$\alpha\beta\gamma\delta\zeta$
199	6373.81	Lyα	4.24304	0.00179	123	208	13.91	0.79	0.38	0.20	α
200	6377.82	Lyα	4.24634	0.00015	78	11	15.27	0.05	1.16		$\alpha\beta\gamma$
201	6380.16	Lyα	4.24826	0.00007	20	6	14.61	0.14	0.29		$\alpha\beta\gamma$
202	6382.30	Lyα	4.25002	0.00005	33	6	14.72	0.28	0.46		$\alpha\beta\gamma$
203	6386.45	Lyα	4.25344	0.00018	148	22	14.00	0.05	0.46		α
204	6390.92	Lyα	4.25712	0.00006	16	4	13.45	0.10	0.10	0.34	α
205	6391.82	Lyα	4.25785	0.00003	15	3	14.13	0.18	0.19		$\alpha\beta$
206	6395.35	Lyα	4.26076	0.00003	66	3	15.22	0.10	0.99		$\alpha\beta$
207	6399.38	Lyα	4.26407	0.00003	20	3	13.38	0.05	0.10		α
208	6403.23	Lyα	4.26724	0.00013	67	11	13.49	0.06	0.15	0.03	α
209	6406.83	Lyα	4.27020	0.00007	41	6	13.41	0.05	0.12		α
210	6412.13	Lyα	4.27456	0.00006	28	2	14.83	0.08	0.42	0.20	$\alpha\beta\gamma$
211	6413.26	Lyα	4.27549	0.00003	9	1	16.12	0.21	0.21		$\alpha\beta\gamma\kappa\lambda$
212	6414.59	Lyα	4.27658	0.00003	19	4	14.50	0.36	0.27		α
213	6416.20	Lyα	4.27791	0.00002	17	2	13.62	0.05	0.13		α
214	6419.52	Lyα	4.28064	0.00006	13	6	12.82	0.12	0.03	0.16	α
215	6420.63	Lyα	4.28155	0.00003	12	2	13.29	0.07	0.07		α
216	6421.67	Lyα	4.28241	0.00007	13	8	12.76	0.15	0.03		α
217	6422.84	Lyα	4.28337	0.00021	41	25	13.07	0.26	0.06	0.22	α
218	6424.48	Lyα	4.28472	0.00003	17	3	14.03	0.17	0.20		α
219	6427.44	Lyα	4.28715	0.00004	22	4	13.95	0.13	0.21		α
220	6427.50	Lyα	4.28720	0.00019	139	32	14.07	0.05	0.51		α
221	6433.08	Lyα	4.29179	0.00029	39	7	16.17	0.16	0.80		$\alpha\iota$
222	6435.11	Lyα	4.29347	0.00008	30	8	15.32	0.30	0.51		$\alpha\beta$
223	6436.58	Lyα	4.29468	0.00069	46	33	13.72	0.50	0.22		α
224	6438.48	Lyα	4.29624	0.00002	18	2	13.67	0.05	0.14	0.77	α
225	6440.90	Lyα	4.29823	0.00002	20	1	14.90	0.13	0.31		$\alpha\beta$
226	6444.75	Lyα	4.30139	0.00007	75	6	14.10	0.03	0.46	0.23	α
227	6447.67	Lyα	4.30380	0.00003	20	2	14.69	0.14	0.30		$\alpha\beta$
228	6452.06	Lyα	4.30741	0.00021	90	9	14.86	0.05	1.09		$\alpha\beta$
229	6454.21	Lyα	4.30918	0.00004	29	4	15.06	0.07	0.47		$\alpha\beta\gamma$
230	6456.38	Lyα	4.31096	0.00011	34	9	14.46	0.10	0.41		$\alpha\beta$
231	6457.62	Lyα	4.31198	0.00003	15	2	15.42	0.21	0.29		$\alpha\beta\delta$
232	6459.07	Lyα	4.31317	0.00007	28	4	14.07	0.06	0.28		$\alpha\beta$
233	6463.34	Lyα	4.31668	0.00007	31	5	13.61	0.07	0.16	0.94	α
	6472– 6504 not covered										
234	6506.81	Lyα	4.35244	0.00009	82	8	14.37	0.05	0.69	0.08	$\alpha\beta$
235	6511.10	Lyα	4.35597	0.00007	45	9	14.46	0.13	0.51	0.97	α
236	6513.70	Lyα	4.35811	0.00074	120	45	14.05	0.19	0.48		α
237	6518.23	Lyα	4.36184	0.00003	34	4	14.31	0.10	0.38		$\alpha\beta$
238	6520.91	Lyα	4.36405	0.00003	22	1	16.26	0.08	0.48		$\alpha\beta\gamma\delta\epsilon\zeta\theta\iota$
239	6522.34	Lyα	4.36522	0.00009	31	3	15.01	0.08	0.49		$\alpha\beta\gamma$
240	6527.28	Lyα	4.36928	0.00007	68	6	13.86	0.03	0.30	0.95	α
241	6530.69	Lyα	4.37208	0.00024	44	17	13.44	0.17	0.13		α
242	6532.08	Lyα	4.37323	0.00003	23	2	14.42	0.09	0.30		$\alpha\gamma$
243	6538.49	Lyα	4.37850	0.00004	45	3	14.49	0.07	0.52	0.28	$\alpha\beta$
244	6540.22	Lyα	4.37993	0.00003	7	4	13.25	0.14	0.06		$\alpha\beta$
245	6541.48	Lyα	4.38097	0.00005	33	6	13.77	0.06	0.21		$\alpha\beta$
246	6543.45	Lyα	4.38259	0.00016	44	23	13.27	0.18	0.09		$\alpha\beta$
247	6545.59	Lyα	4.38434	0.00003	32	3	14.25	0.07	0.34		$\alpha\beta$
248	6547.39	Lyα	4.38583	0.00005	11	6	12.82	0.12	0.03		$\alpha\beta$
249	6549.14	Lyα	4.38727	0.00002	34	2	14.35	0.07	0.39		$\alpha\beta$
250	6552.17	Lyα	4.38976	0.00002	34	2	14.28	0.05	0.37		$\alpha\beta$
251	6554.35	Lyα	4.39155	0.00005	17	5	12.96	0.08	0.04		α
252	6557.31	Lyα	4.39399	0.00003	49	3	14.47	0.04	0.55	0.50	$\alpha\beta$
253	6559.55	Lyα	4.39583	0.00004	20	2	13.38	0.04	0.10		α
254	6561.76	Lyα	4.39764	0.00002	19	2	13.66	0.05	0.15	0.03	α

1994ApJ...428..574W

TABLE 1—*Continued*

n	$\lambda_{\rm vac}$		ID	z	±	b	±	$\log N$	±	w_λ	p	Comments
255	6564.75	│	Lyα	4.40011	0.00003	30	3	13.66	0.03	0.17	0.05	α
256	6566.68	│	Lyα	4.40169	0.00003	28	2	13.71	0.04	0.18		α
257	6568.13	│	Lyα	4.40289	0.00004	9	4	12.85	0.09	0.03		α
258	6569.49	│	Lyα	4.40401	0.00009	16	8	12.61	0.16	0.02		α
259	6573.48	│	Lyα	4.40729	0.00004	45	3	13.98	0.03	0.32	0.97	α
260	6575.35	│	Lyα	4.40882	0.00002	19	1	15.29	0.10	0.33		$\alpha\beta\gamma\epsilon$
261	6576.69	│	Lyα	4.40993	0.00002	10	2	13.04	0.05	0.05		α
262	6579.71	│	Lyα	4.41241	0.00006	27	3	14.32	0.11	0.33	0.68	α
263	6580.83	│	Lyα	4.41333	0.00012	21	5	13.53	0.18	0.12		α
264	6585.65	│	Lyα	4.41730	0.00003	24	2	14.23	0.07	0.28	0.15	$\alpha\beta$
265	6587.97	│	Lyα	4.41921	0.00003	35	3	15.09	0.17	0.55		$\alpha\beta\gamma$
266	6590.76	│	Lyα	4.42150	0.00022	56	24	13.67	0.18	0.21		α
267	6592.20	│	Lyα	4.42269	0.00004	26	3	13.82	0.10	0.20		α
268	6596.76	│	Lyα	4.42643	0.00015	36	3	14.29	0.24	0.39	0.22	$\alpha\beta\gamma$
269	6597.16	│	Lyα	4.42677	0.00006	22	3	14.98	0.12	0.35		$\alpha\beta\gamma$
270	6601.01	│	Lyα	4.42993	0.00001	23	2	14.32	0.09	0.28	0.74	α
271	6602.69	│	Lyα	4.43131	0.00004	25	3	13.30	0.04	0.09		α
272	6604.30	│	Lyα	4.43264	0.00003	22	3	13.17	0.05	0.07		α
273	6606.74	│	Lyα	4.43464	0.00006	57	5	13.55	0.03	0.16		α
274	6609.49	│	Lyα	4.43690	0.00003	2	8	12.87	2.04	0.02	0.03	α
275	6610.77	│	Lyα	4.43796	0.00001	21	1	14.14	0.05	0.24		$\alpha\beta$
276	6612.69	│	Lyα	4.43954	0.00002	22	1	13.94	0.04	0.21		$\alpha\beta$
277	6613.68	│	Lyα	4.44036	0.00003	2	1	13.49	0.49	0.03		$\alpha\beta$
278	6614.28	│	Lyα	4.44085	0.00006	16	6	13.69	0.14	0.14		$\alpha\beta$
279	6615.46	│	Lyα	4.44182	0.00005	24	3	14.53	0.07	0.33		$\alpha\beta$
280	6618.71	│	Lyα	4.44449	0.00008	52	4	15.46	0.07	0.87		$\alpha\beta\gamma\delta\epsilon$
281	6621.48	│	Lyα	4.44677	0.00004	20	1	15.41	0.09	0.36		$\alpha\beta\gamma\delta\epsilon$
282	6623.42	│	Lyα	4.44836	0.00002	20	1	14.54	0.07	0.28		$\alpha\beta$
283	6624.40	│	Lyα	4.44917	0.00003	5	3	13.35	0.18	0.05		$\alpha\beta$
284	6624.92	│	Lyα	4.44960	0.00007	17	4	13.23	0.10	0.07		$\alpha\beta$
285	6627.40	│	Lyα	4.45164	0.00008	49	7	13.29	0.05	0.10	0.16	$\alpha\beta$
286	6629.69	│	Lyα	4.45352	0.00004	19	2	13.97	0.08	0.20		$\alpha\beta$
287	6631.07	│	Lyα	4.45466	0.00004	27	2	14.33	0.08	0.33		$\alpha\beta$
288	6633.36	│	Lyα	4.45655	0.00001	18	1	13.84	0.04	0.17		$\alpha\beta$
289	6636.17	│	Lyα	4.45885	0.00008	89	7	13.79	0.03	0.28		α
290	6640.16	│	Lyα	4.46213	0.00002	25	2	14.16	0.06	0.27		α
291	6642.19	│	Lyα	4.46380	0.00005	38	4	13.69	0.07	0.19		α
292	6643.50	│	Lyα	4.46489	0.00035	62	22	13.23	0.20	0.09		α
293	6646.80	│	Lyα	4.46760	0.00002	27	2	13.91	0.03	0.23	0.51	$\alpha\beta$
294	6648.39	│	Lyα	4.46890	0.00006	21	6	13.12	0.09	0.06		$\alpha\beta$
295	6649.89	│	Lyα	4.47014	0.00005	25	4	13.39	0.05	0.10		$\alpha\beta$
296	6651.40	│	Lyα	4.47138	0.00006	15	5	12.84	0.10	0.03		α
297	6654.31	│	Lyα	4.47377	0.00004	38	3	13.82	0.03	0.24	0.31	α
298	6657.16	│	Lyα	4.47612	0.00006	30	5	13.35	0.06	0.10		α
299	6660.54	│	Lyα	4.47890	0.00007	25	7	13.26	0.08	0.08		α
	6663 – 6701 not covered											
300	6705.45		OI1302?	4.14945	0.00005	32	4	13.99	0.05	0.06	0.90	
301	6710.25		OI1302?	4.15314	0.00006	30	5	13.74	0.06	0.04	1.00	
302	6712.86		OI1302?	4.15515	0.00003	24	2	14.12	0.03	0.08	0.30	
303	6738.47		OI1302?	4.17481	0.00002	11	2	14.02	0.04	0.06	0.08	
	6858 – 6910 not covered											
304	6981.32		CIV1548	3.50933	0.00003	21	3	13.50	0.05	0.10	0.58	
305	6992.95		CIV1550	3.50933	0.00003	21	3	13.50	0.05	0.06	0.58	
	7071 – 7131 not covered											
306	7228.21	│	CIV1548	3.66880	0.00005	41	5	13.69	0.04	0.17	0.01	
307	7231.64	│	CIV1548	3.67102	0.00006	39	5	13.60	0.05	0.14		
308	7234.61	│	CIV1548	3.67294	0.00009	29	8	13.22	0.10	0.06		Possible
309	7236.82	│	CIV1548	3.67436	0.00004	15	4	13.21	0.08	0.06		
310	7240.25	│	CIV1550	3.66880	0.00005	41	5	13.69	0.04	0.09		
311	7243.03	│	CIV1548	3.67839	0.00011	55	10	13.61	0.07	0.15		Doubtful
312	7243.69	│	CIV1550	3.67102	0.00006	39	5	13.60	0.05	0.07		
313	7255.13		CIV1550	3.67839	0.00011	55	10	13.61	0.07	0.08	0.01	Doubtful
	7300 – 7372 not covered											

NOTES.—Vertical bars indicate blended features. The fit probability p applies for the whole blend, plus any higher order lines fitted. The lines which were used to constrain the fits are indicated by the appropriate Greek letters in the comments column. The $\omega\lambda$ are rest equivalent widths derived from the fitted log N and b values.

and are fitted as a single component at $z = 3.67086$ and log $N_{\rm H\,I} = 19.14$. No other confirming lines were found. The Lyα absorption is strong for the $z = 3.66880$, 3.67102, and 3.67294 components. It did not prove possible to deblend the Lyα to obtain component-by-component column densities with any useful precision, but it is likely that the value log $N_{\rm H\,I} = 19.14$ is an overestimate for the sum of the systems. If we constrain the Lyα components to have the same redshifts and Doppler parameters as the C IV lines, then the best estimate for the total is log $N_{\rm H\,I} \sim 18.1$, with the major contribution from $z = 3.67294$. If more Lyα components are present, then the total H I column density could be even lower. The reality of the highest redshift component $z = 3.67839$ is very doubtful, since each of the possible C IV lines lies under night-sky emission and the corresponding Lyα is not detectable.

3.3. *The* $z = 4.16$ *System*

This system is based mainly on the presence of Lyman limit absorption at 4738 Å and a damped Lyα at 6279 Å ($z \sim 4.165$) in the low-resolution data. The observed Lyman limit at the Lyα redshift falls at 917.3 Å in the rest frame, i.e., longward of the 912 Å Lyman limit wavelength. The difference is probably due to velocity structure and the blending of high-order Lyman lines shifting the Lyman edge redward.

The red wing of the Lyα feature is not covered in the echelle spectrum, so it is not possible to determine an accurate redshift or a reasonable H I column density estimate. From a fit to the low-resolution Lyα against a local continuum allowing for the average Lyα forest, the total H I column density is unlikely to be much greater than 3×10^{20} cm^{-2}. Two commonly seen heavy-element lines (O I 1302 and Si II 1304) would fall in the spectral region around 6705–6745 Å in the long-wavelength wing of the Lyα emission line, and four absorption features are seen in this region. None of the wavelength ratios for these lines corresponds to that for Si II 1304:O I 1302, so we tentatively identify all four as O I 1302. Unfortunately, we are unable to confirm these identifications since the other common lines are either lost in the Lyα forest or fall in spectral regions which were not covered. Therefore, while at least some of the features in the range 6705–6740 Å are likely to arise from O I, it is not necessarily true that all do. In fact, the feature at 6712.9 Å, which could be identified with O I 1302 with log $N_{\rm O\,I} = 14.1$, would then have a corresponding H I with log $N_{\rm H\,I} \leq 17.5$. This would give at least a solar oxygen abundance, a conclusion which we are reluctant to accept without some other supporting evidence. Further data covering C II 1334 and the long-wavelength wing of Lyα at this redshift are needed before this system can be analyzed.

4. THE Lyα FOREST

The signal-to-noise ratio (S/N) in the spectrum falls off at either end of each of the orders, and our ability to deblend complex features depends on the S/N. As a consequence, the full line list given in Table 1 does not provide a well-defined sample. To obtain such a sample of Lyα lines, we select those regions for which the S/N > 4.5 per 0.055 Å pixel. We estimate the 5 σ detection limit to be log $N_{\rm H\,I} = 13.3$ for Lyα lines with $b = 60$ km s^{-1} at this S/N. Derived distributions are based on a sample of 183 lines with log $N_{\rm H\,I} > 13.3$ with redshifts set by the S/N criterion. The redshift ranges for the sample are $z = 3.7000$–3.7710, 3.7916–3.8944, 3.9191–4.0301, 4.0548–4.1412, and 4.1988–4.3139. Lines in the highest redshift range ($4.3502 < z < 4.4809$) are sufficiently close to that of the QSO that the proximity effect may be important (Lu et al. 1991), so these are excluded from the analyses unless otherwise stated.

This detection limit quoted is for isolated lines. In practice, because of the well-known increase of the Lyα line density with redshift, there is so much line blending in the spectrum of QSO BR 1033−0327 that many weak lines go undetected. It is difficult to determine the correction factor for this effect. The best method would be to analyze simulated spectra in the same way as the real data, trying a range of different assumed input parameter distributions. This is a major project and beyond the scope of the present paper. To obtain an estimate of the effect of the stronger lines on the raw detection probability of the weaker ones, we have randomly added weak artificial lines to the spectrum and noted the fraction which would be found. In the wavelength range 6330–6450 Å, we find that when we insert Lyα lines with $b = 30$ km s^{-1} and log $N_{\rm H\,I} = 13.7$, approximately 25% of the added lines are clearly visible and 40% of the lines are lost completely in strong features. The remaining 35% affect the line profiles of the stronger features and may be detectable when the profiles are fitted with higher order Lyman lines included. Thus the true number of systems with H I column densities around log $N_{\rm H\,I} = 13.7$ is likely to be 2–4 times higher than the number we have found. This has obvious implications for the H I column density distribution and for inferences concerning the redshift evolution of the number of systems.

4.1. *Parameter Distributions*

4.1.1. *Doppler Parameters*

The Doppler parameter distribution is shown in Figure 4 (*upper*). The distribution here is considerably broader than similar distributions derived from lower redshift data (Carswell et al. 1991a; Rauch et al. 1992, 1993) shown in Figure 4 (*lower*). The excess of high Doppler parameter systems at higher redshifts is likely to be due to our failure to deblend some of the complexes, so we do not regard their presence as indicating significant intrinsic differences between the distributions at the different redshifts. However, there is a marked excess of systems $15 < b < 20$ km s^{-1} at high redshifts, with about 20% of the 183 lines having Doppler parameters below 22 km s^{-1}. This compares with 10% of 240 lines in the lower redshift sample.

With a large number of unresolved blends likely to cause an apparent excess at large Doppler parameters, the median or the mean of the number distribution will not be useful for determining the characteristic b. A more useful measure is likely to be position of the peak of the distribution, though this quantity is not well-defined for the distributions we have here. For the BR 1033−0327 data, the peak is in the range 18–28 km s^{-1}. For Lyα absorption systems in the redshift range $1.86 < z < 3.27$ in our data set (see Fig. 4), the peak is broader, covering 23–36 km s^{-1}. Typical values in the peak are ~5 km s^{-1} higher. If we exclude lines with $b > 45$ km s^{-1} as being probably unresolved blends, then the Kolmogorov-Smirnov probability that the data sets covering $1.86 < z < 3.27$ and $3.7 < z < 4.3$ arise from the same distribution is 10^{-3}.

There are two ways in which differences between the two distributions could arise even if they were intrinsically similar. One possibility is that the Doppler parameters in the higher redshift sample have larger errors than those in the lower redshift sample. The Doppler parameter distribution would be broader at high redshifts simply because of increased scatter.

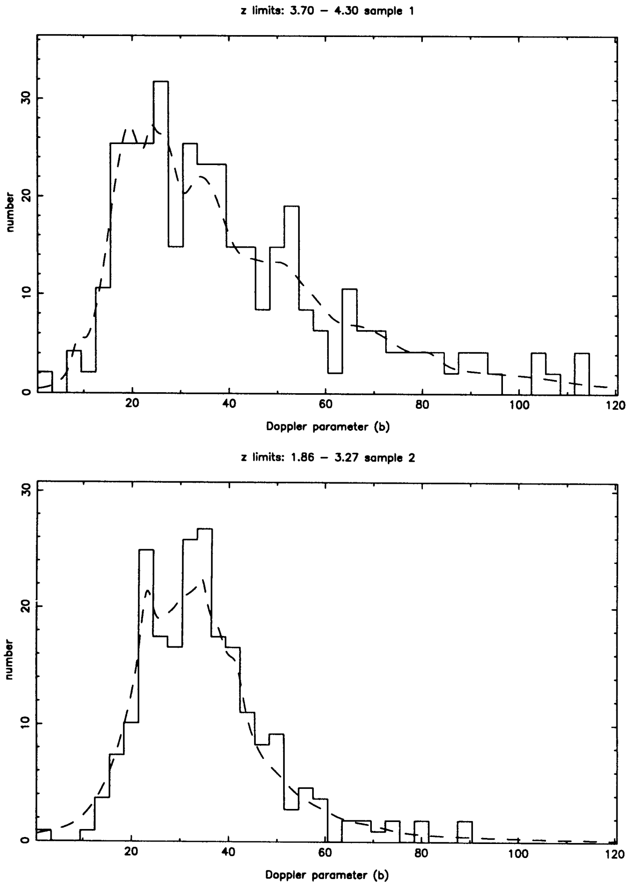

FIG. 4.—*Upper*, Doppler parameter distribution for $3.7 \leq z \leq 4.3$. Values of $b > 45$ km s^{-1} could well arise from unresolved blends. There is a marked excess of systems with $15 < b < 20$ km s^{-1} compared to lower z data. The dashed curves show the distribution as a sum of Gaussians based on the estimated Doppler parameters and their error estimates (see text for details). *Lower*, Doppler parameter distribution for $1.86 < z < 3.27$. If both data sets are truncated to eliminate lines with $b > 45$ km s^{-1}, the probability that the two data sets arise from the same parent distribution is 0.001.

To check that this is not a significant effect, we have constructed continuous Doppler parameter distributions by adding Gaussians centered on the individual b value estimates with σ values equal to the error estimates. The results are shown as dashed curves in Figure 4. If errors in the b values give rise to significant broadening of the distributions, then these smooth curves should be even broader than the histograms. It is evident that they are not, so the distributions are not significantly affected by errors in the Doppler parameters.

The second possibility is that the difference might arise in a subtle way as a result of our attempting to fit minimum numbers of velocity components to blended features. If, for example, we are fitting a complex which contains two strong components with a weaker one in one of the wings of the feature, we may find that the fitting criterion requires only a single, broader strong component along with a weaker line in the wing. Under these circumstances, the fitted strong component will have a larger Doppler parameter than either of the true systems which underlie it and so will generally have broader wings than exist in reality. As a consequence, any lines in these wings would appear to be weaker, and narrower, than they are in reality. The overall result would be an inferred mixture of lines with components broader and narrower than are really there. It is difficult to address this point without fitting simulated data, but we note that there is no evidence that the narrow lines are preferentially associated with broad ones. Other data sets with comparable (but lower) resolution, which consistently use more than one Lyman series line for profile fitting, are those of Carswell et al. (1987) and Rauch et al. (1992), both of whom use similar profile-fitting methods. They do not find a similar excess of low b values, so it seems likely that the excess found here is real.

4.1.2. H I *Column Densities*

The raw H I column density distribution is shown in Figure 5. Unlike the $N_{\rm H\,I}$ distributions derived from similar samples at lower redshifts (Rauch et al. 1993, and references therein), it is not well fitted by a power law for H I column densities above the detection limit, $\log N_{\rm H\,I} > 13.3$. The probability that a power-law distribution yields the observed data is only 4×10^{-3}, with best-fit parameters $d\mathcal{N}/dN_{\rm H\,I} \propto N_{\rm H\,I}^{-\beta}$, $\beta = 1.45 \pm 0.03$. However, given the great uncertainty about the number of weak lines which have been missed, we cannot say that a steeper power law is really excluded. The index found at lower redshifts where line blending is less of a problem, $\beta = 1.7$ (Rauch et al. 1993), is consistent with the distribution for $\log N_{\rm H\,I} > 14.5$. If we extrapolate this power law to $\log N_{\rm H\,I} = 13.7$, then the number of systems per unit H I column density is about 3 times higher than the number found. Since, as discussed above, we are probably measuring only 25%–50% of the systems at that column density, a single power law with $\beta = 1.7$ could well be the correct fit.

4.1.3. *Correlations*

An independent check of the number of weak lines (and thus of the possible applicability of the $\beta = 1.7$ power law) comes from comparing the total flux removed from the QSO spectrum with the predictions from simulated spectra made using different $N_{\rm H\,I}$ and b distributions. We assume that the distributions of *both* $N_{\rm H\,I}$ and b are the same as at lower redshifts, as for the Rauch et al. (1993) simulations, and normalize to the number of systems found with $\log N_{\rm H\,I} > 14.5$ (because few of

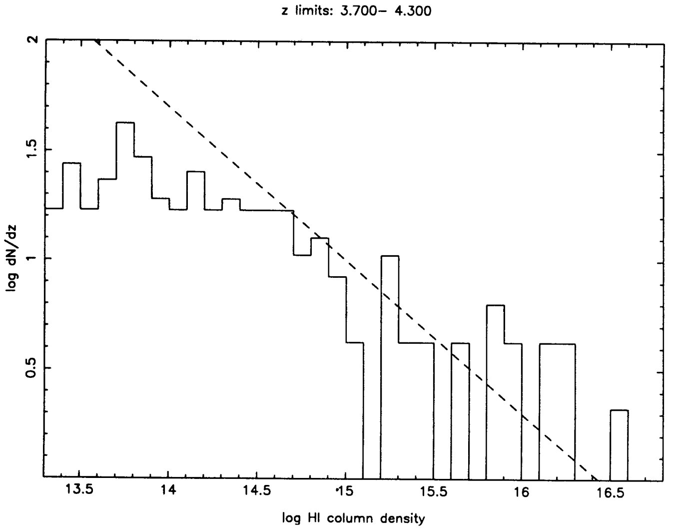

FIG. 5.—H I column density distribution for $3.7 \leq z \leq 4.3$. A simple power law does not fit the data. However, weak lines are lost to blending, and a power-law fit consistent with lower z data, $d\mathcal{N}/dN_{\rm H\,I} \propto N_{\rm H\,I}^{-\beta}$, $\beta \approx 1.7$ (*dashed line*), is not ruled out.

these should be lost). Then, for randomly distributed lines with Doppler parameters drawn from a normal distribution with mean $b = 25$ km s^{-1} and standard deviation $\sigma = 5$ km s^{-1} truncated at zero, the average residual flux in the Lyα forest at $z = 4.2$ is 0.31 times the continuum. This disagrees with the observed value of 0.37 times the continuum. The two ways to remove this discrepancy are to change the $N_{\rm H\,I}$ distribution and/or to change the Doppler b distribution. We have tried keeping the same $N_{\rm H\,I}$ power law while using other mean Doppler parameters with the same σ and have found that a mean b in the range 15–20 km s^{-1} gives the observed average residual intensity. Since this is similar to the observed shift in the *peak* of the b distribution as compared to the lower redshift data, we conclude that, in fact, it is consistent to assume that the slope of the $N_{\rm H\,I}$ distribution is unchanged and that only the b distribution is different.

In all the above simulations, though, the spectra look somewhat different from that of the object, in that the simulations produce lines which seem to be more evenly spaced and velocity components which are more easily separated. A way of quantifying this difference is to look at the number of regions of spectrum above 50% of the continuum over some wavelength range. For a noise-free spectrum generated from the data in the Lyα forest in order 35, there are 20 such regions. For the simulated data, this value is $\sim$30. One obvious way this difference could occur is if the Lyα systems are not distributed randomly, e.g., if they are clustered. However, the two-point correlation function for all systems with log $N_{\rm H\,I} > 13.3$ shows no signal down to splittings of $\Delta v = 50$ km s^{-1} (Fig. 6). The same result applies for systems with log $N_{\rm H\,I} > 14.3$, so strong clustering does not provide the explanation for the appearance of the spectrum. This is consistent with the result by Rauch et al. (1992) for their entire data set.

This leaves us without any real understanding of why the spectrum looks as it does. An obvious possibility is that the distribution of Doppler parameters has an extended tail toward larger values and that our assumption that this tail is largely due to unresolved blends is incorrect. The presence of such an extended tail in the underlying Doppler parameter distribution is indicated by the elegant analysis of a sample of QSOs by Press & Rybicki (1993). This question should be explored using data simulations for various distribution functions and correlation functions and fitting these simulations, as was done here for BR 1033−0327. This may form the subject of future investigation, if the profile fitting of several Lyman series lines in these highly blended spectra can be adequately automated.

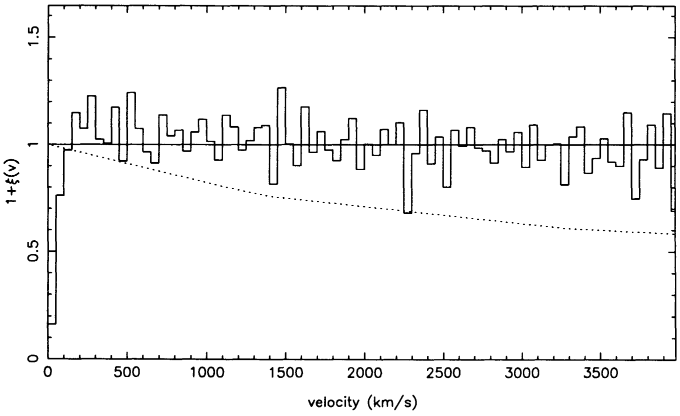

FIG. 6.—Two-point correlation function at $3.7 \le z \le 4.3$ for all systems with log $N_{\rm H\,I} > 13.3$. The dotted curve is the renormalization introduced to compensate for incomplete spectral coverage. There is no significant signal down to velocity splittings of $\Delta v \sim 100$ km s^{-1}.

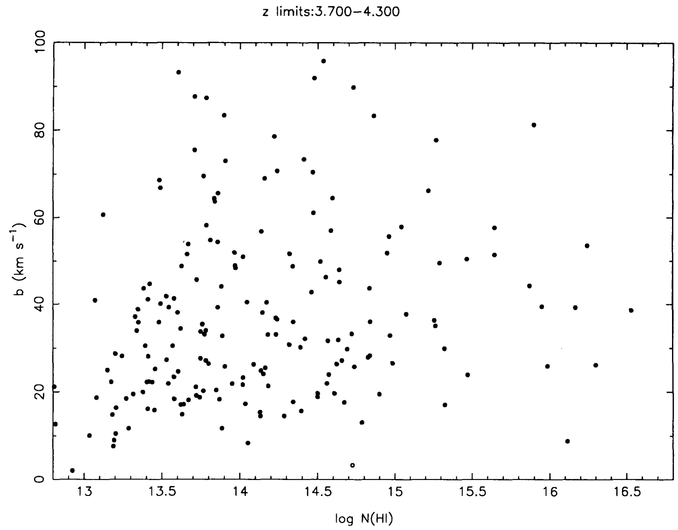

FIG. 7.—b vs. $N_{\rm H\,I}$ distribution for $3.7 \le z \le 4.3$. The correlation coefficient between b and log $N_{\rm H\,I}$ is 0.006, with a probability of 0.93 that the two quantities are uncorrelated.

The correlation coefficient between b and log $N_{\rm H\,I}$ is 0.006, with a probability of 0.93 that the two quantities are uncorrelated (Fig. 7). The high Doppler parameters from possible unresolved blends could mask a correlation, if one exists, but would be unlikely to do so completely if the correlation is as strong as the one proposed by Pettini et al. (1990). This lack of correlation is consistent with the results at lower redshifts of Carswell et al. (1991a) and Rauch et al. (1992, 1993).

4.2. *Redshift Dependence*

To estimate the redshift dependence of the number of Lyα systems per unit redshift, we combine these new results from the BR 1033−0327 observations with those from the lower redshift objects 1101−264 (Carswell et al. 1991a), 2206−199 (Rauch et al. 1993), and 0014+813 (Rauch et al. 1992). This gives a redshift baseline covering $1.86 < z < 4.3$. For systems with log $N_{\rm H\,I} > 13.3$ and for an assumed single-power-law fit to the numbers per unit redshift of the form $d\mathcal{N}/dz \propto (1+z)^{\gamma}$, the redshift evolution index $\gamma = 2.0 \pm 0.3$. However, as discussed above, many of the low $N_{\rm H\,I}$ systems will be lost in blends at the highest redshifts, so this is likely to be an underestimate of the true number evolution. If we confine our attention to systems with log $N_{\rm H\,I} > 14.5$, where blending is less of a problem, then for $1.86 < z < 4.3$ we find $\gamma = 4.6 \pm 0.7$, with a probability 0.90 that such a power law describes the data (Fig. 8). This is considerably steeper than previous estimates at lower redshifts (e.g., Lu et al. 1991, $\gamma = 2.75 \pm 0.29$ over the redshift range $1.7 < z < 3.8$; Morris et al. 1991, $\gamma = 0.8 \pm 0.4$ for $0 < z < 2.1$).

If a single H I column density distribution applies over the whole redshift range $1.86 < z < 4.3$, then the best fit may be a broken power law, since the three low redshift objects taken together yield $\gamma = 3.1 \pm 0.5$ for log $N_{\rm H\,I} > 13.3$ (2.5 ± 1.5 for log $N_{\rm H\,I} > 14.5$) and 0014+813 and BR 1033−0327 together yield $\gamma = 5.5 \pm 1.1$ for log $N_{\rm H\,I} > 14.5$. Thus, there appears to

1994ApJ...428..574W

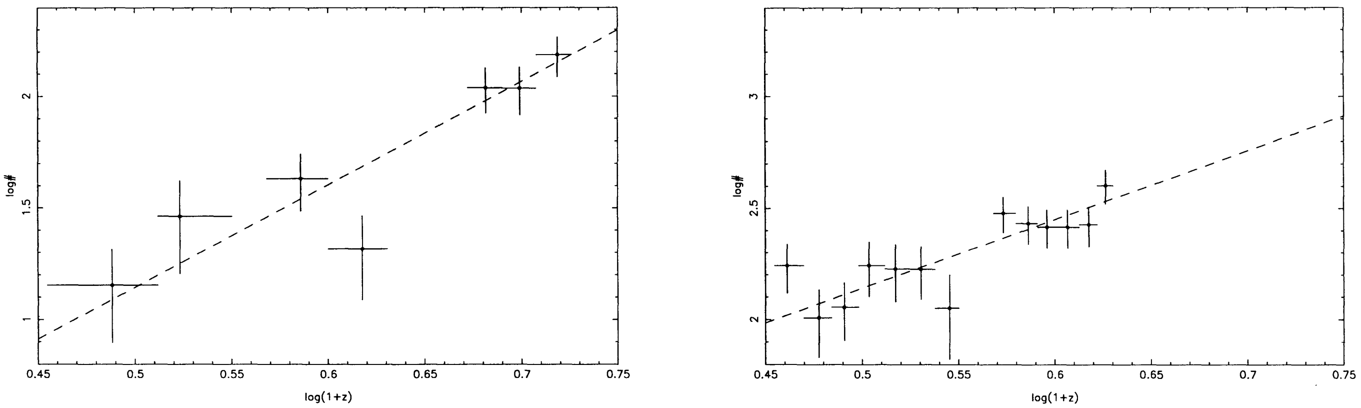

FIG. 8.—Redshift distribution for $1.86 \leq z \leq 4.3$. The single-power-law fit for systems with $\log N_{\rm H\,I} > 14.5$ (*left*) is $d\mathcal{N}/dz \propto (1+z)^{\gamma}$, $\gamma = 4.6 \pm 0.7$, with a probability of 0.74 that such a power law describes the data. This is steeper than any lower z determination. For comparison, the redshift dependence for systems with $\log N_{\rm H\,I} > 13.3$ over the redshift range $1.86 \leq z \leq 3.27$ is shown to the same relative scale in the *right* panel. Note that the $\log N_{\rm H\,I} > 14.5$ limit at high z, necessary to avoid blending effects, affects the bin size.

be a steepening of the redshift evolution of the Lyα systems at the highest redshifts for the strongest lines, and possibly for weaker lines as well.

At first sight, this result appears to contradict those of Irwin et al. (1991) and Press, Rybicki, & Schneider (1993), who find that a single power law fits over the whole redshift range. However, both studies used the average Lyα forest depression technique (Oke & Korycansky 1982), which relates more directly to changes in average Lyα equivalent width than to those in H I column density. For our high column density limit, the Lyα lines are on the logarithmic part of the curve of growth, where the equivalent width changes little for substantial changes in H I column density. Under these circumstances, changes in the redshift evolution would be evident only from high-resolution data such as those presented here. Interestingly, the analysis of Zuo & Lu (1993), which used a version of the average Lyα depression method, suggests a broken power law with indices similar to those given here.

We cannot address in detail the question as to whether the number-redshift relation depends on the H I column density. However, we note that if there is a column-density–dependent redshift evolution of the numbers of systems, then the shape of the H I column density distribution must change with redshift. Since the considerations discussed above suggest that a single power law could fit the H I column density distribution at all redshifts, the results here indicate that the number evolution may be independent of H I column density.

4.3. *Proximity Effect*

It was noted above that the redshift range covered in echelle order 34, corresponding to $4.351 < z < 4.474$, was omitted because of its proximity to the QSO redshift. We can use the measurements in this order to estimate the background ionizing flux at $z \sim 4.2$. We compare the H I column densities in systems in this echelle order with those at lower redshifts and assume that any differences arise from the differences in the known ionizing flux emitted by the QSO.

The derivation of the form of the effect is straightforward: if we assume that the clouds are highly ionized, that the clouds' proximity to the QSO does not significantly affect the clouds' density or temperature, and that the QSO spectral index is the same as that of the background radiation, then for a cloud which would have H I column density $N_{\rm H\,I}$ far from the QSO, the H I column density at redshift z_a is

$$N'_{\rm H\,I} = N_{\rm H\,I}\,\frac{f_b}{f_q + f_b}\,,$$

where f_q is the flux due to the QSO and f_b is the background flux. For a $q_0 = \frac{1}{2}$ cosmology, and a QSO redshift z_e,

$$f_q = f_0\,\frac{(1 + z_e - \sqrt{1 + z_e})^2(1 + z_a)^3}{(1 + z_e)(R - \sqrt{R})^2}\,,$$

where $R = (1 + z_e)/(1 + z_a)$ and f_0 is the observed flux at the wavelength of the redshifted Lyman limit at the Earth. In this case, $f_0 = 8.0 \times 10^{-28}$ ergs cm^{-2} s^{-1} Hz^{-1} and the emission redshift $z_e = 4.506$.

We took the measured redshifts of the lines with measured column densities in orders 37 and 35 and added a constant so that they would span order 34 (implicitly assuming that the number of systems per unit redshift is constant over the redshift range of interest). We then applied a correction to the H I column densities at the new redshifts based on the equation above, with the assumption that the background flux f_b is constant over the redshift range of interest, $3.9 \lesssim z \lesssim 4.5$. To determine an estimate for f_b, we compared the average residual intensity with that actually found for order 34. The estimates from the two different base regions differ by about 0.2 dex, with an average $f_b = 4 \times 10^{-21}$ ergs cm^{-2} s^{-1} Hz^{-1}. Thus $J_\nu = f_b/4\pi = 3 \times 10^{-22}$ ergs cm^{-2} s^{-1} Hz^{-1} sr^{-1}.

Since the number density of Lyα systems increases steeply with redshift, the number density of systems near the QSO may have been underestimated in the above calculation. If this is true, then the QSO must have an even greater effect on the H I column densities, so the background that we determine would be an overestimate. The redshift differences between the chosen background range (orders 35 and 37) and the region near the QSO redshift (order 34) are small, so this should not be a large effect. Tests in which we change the line density to account for this evolution show that it lowers our estimate of the background by about 10%.

An additional source of error arises from the uncertainty in the true emission redshift of BR 1033−0327, which was determined primarily from the C IV 1549 emission line. Espey et al. (1989) found an average velocity blueshift of ∼1000 km s^{-1} of the high-ionization emission lines with respect to the low-ionization lines in QSOs with redshifts $z \sim 2$, and subsequent attempts to measure the true redshift using forbidden lines indicates that the systemic redshift is closer to that of the low-ionization lines (Carswell et al. 1991b). If we suppose that the systemic redshift of BR 1033−0327 is 1000 km s^{-1} higher than the C IV measurement indicates at $z = 4.524$, then we find J_ν decreases to $\sim 1.3 \times 10^{-22}$ ergs cm^{-2} s^{-1} Hz^{-1} sr^{-1}.

Thus, we estimate that the background flux at the midrange redshift $z \sim 4.2$ is in the range $10^{-22} \lesssim J_\nu \lesssim 3 \times 10^{-22}$ ergs cm^{-2} s^{-1} Hz^{-1} sr^{-1} at the Lyman edge. While this estimate should be reasonably reliable, it is based on comparing results with those from a single spectral region near the Lyα emission line, so confirmation from at least one other object is desirable.

Our estimate of the background flux at $z \sim 4.2$ is lower than the value $J_\nu \sim 10^{-21}$ or more found at redshifts $z \sim 2.5$ (Bajtlik, Duncan, & Ostriker 1988; Lu et al. 1991; Parnell 1989; Bechtold 1994). Models computed by Madau (1992) show that this level of background flux could arise from QSOs alone if they have constant comoving density at redshifts $z \gtrsim 2$ (Irwin et al. 1991) and if their flux is attenuated by Lyman limit systems. However, in this and most other models, the QSOs fail to account for all the background radiation inferred at redshifts $z \sim 2.5$ (see Miralda-Escudé & Ostriker 1990). If the emission is dominated by galaxies at $z \sim 2.5$, then most of the hot stars in these galaxies must have formed at redshifts $z \lesssim 4$.

4.4. *The Gunn-Peterson Effect*

We can place some approximate limits on the absorption from continuously distributed intergalactic hydrogen by comparing the few small regions of the spectrum with the highest flux values in the Lyα forest with the extrapolated continuum there. The small region at 6408–6410 Å and that centered at 6439.4 Å yield a weighted mean level which is 1.5% below the extrapolated continuum, with an expected error of 3%. The extrapolated continuum error is also about 3%, so if we add these in quadrature, we obtain an error estimate of 5%. This yields a 2 σ estimate that the continuous optical depth at $z \sim 4.3$ is $\tau_{GP} \lesssim 0.1$.

If these regions are representative of Gunn-Peterson absorption, we may infer the intergalactic medium (IGM) density. A convenient formalism is given by Jenkins & Ostriker (1991, eq. [1.3])

$$\tau_{GP} = \frac{1.4 \times 10^{-4}}{J_{-21} h_0} f \left(\frac{\Omega_I}{\Omega_B}\right)^2 (1 + z)^{9/2} ,$$

where $h_0 = H_0/100$ km s^{-1} Mpc^{-1}, J_{-21} is the background flux in units of 10^{-21} ergs cm^{-2} s^{-1} Hz^{-1} sr^{-1} at the Lyman limit, f is a clumping factor, Ω_I is the intergalactic baryon density, and $\Omega_B = (2.02 \pm 0.55) \times 10^{-2} h_0^{-2}$ is the baryon density obtained from nucleosynthesis constraints. We have $J_{-21} = 0.2$, from the discussion above, so for a uniform distribution (where $f = 1$) we find $\Omega_I/\Omega_B < 0.3 h_0^{1/2}$. As Jenkins & Ostriker point out, this limit excludes hot dark matter (HDM) models of the universe and strains cold dark matter (CDM) models.

However, the wavelength regions we used to estimate τ_{GP} are so small that one might argue that these could be regions where the H I density is anomalously low for reasons of density fluctuation or local ionization. To estimate a typical Gunn-Peterson optical depth on this assumption, we compare the extrapolated continuum with an estimate based on local highest flux values and assign the difference between the two to local Gunn-Peterson absorption. We then find that, typically, $\tau_{GP} \sim 0.25$ with occasional voids where the value is lower. In this case, $\Omega_I \sim \Omega_B$ is possible. In principle, this could be checked by attempting to fit the Lyα lines against a lower continuum, relying on the higher order Lyman lines to constrain the fits. We have not done this, but note that, where Lyβ does constrain the fit adequately, the Lyα lines have central intensities close to zero and under these circumstances changes in the continuum level do not have a large effect on the results.

5. DISCUSSION

The most intriguing result from this work is the lower Doppler parameters observed at high redshift. We explore the possibility that the higher redshift clouds are cooler, even though the high b tail of the distribution must still be due to bulk motion (since implausibly high temperatures would otherwise be required; see Baron et al. 1989).

The most obvious explanation for lower temperatures would be the lower background flux at high redshifts. We used the photoionization code CLOUDY (Ferland 1993) to check the magnitude of this effect for a simplified model. We assumed that the density within the clouds is independent of redshift and that the heavy-element abundances are zero. The ionization parameter was set to $U = 5 \times 10^{-3}$, which produces a temperature $T = 2.4 \times 10^4$ K, corresponding to $b = 20$ km s^{-1} (the peak value observed at higher redshift). T is independent of n_e in this regime of U. We then found that, if we increased the ionization parameter by a factor of 5, the temperature increased to $T = 3.4 \times 10^4$ K, corresponding to $b = 25$ km s^{-1} (the low end of the peak range observed at lower redshift). For constant densities, the factor of 5 increase in ionization parameter is equivalent to a factor of 5 increase in ionizing flux. Given the many uncertainties, this is in reasonable agreement with the factor of 3 increase in ionizing flux from $z \sim 4.2$ to $z \sim 2.5$ inferred from the proximity effect. Therefore, the data are consistent with a picture in which the clouds have fairly constant density and are heated by photoionization, and in which the differences in the hydrogen line widths at different redshifts are a consequence of different background fluxes.

An alternative mechanism which would produce a similar temperature change would be for pressure-confined clouds (e.g., Ikeuchi & Ostriker 1986) to expand in response to the factor of ~ 8 decrease in the pressure of an IGM which expands adiabatically between $z = 4.3$ and $z = 2.5$. This density drop by itself would increase the ionization parameter (by the same factor of ~ 8) and cause the cloud temperatures to increase with time, independent of changes in the background ionizing flux.

A third factor which could affect the cloud temperatures would be if He II is ionized at low redshift but not at high redshift, because of high-redshift He II Gunn-Peterson absorption (Miralda-Escudé & Rees 1994). For example, in models with $U > 10^{-2.0}$, $N_{\rm He\,II}/N_{\rm H\,I} > 10$ and a significant component in the thermal balance calculation is energy deposited by He II continuum absorption. If photons with energies greater than 4 ryd do not reach the cloud, then the cloud temperature is lower, with little change to the hydrogen ionization fraction. An example computation using CLOUDY illustrates this. We chose a hydrogen density 10^{-2} and (unabsorbed) log $U = -2.0$, with heavy elements $10^{-4.5}$ solar. He II Gunn-Peterson absorption causes $T_e^{0.5}$ ($\propto b$) to decrease to 0.87 of its former value, consistent with the observed drop to 0.83 of the peak position of the b distribution.

Although Lu et al. (1991) have pointed out important inconsistencies in the proximity effect arguments, we believe that the observed change between $z = 4.2$ and $z = 2.5$ very likely indicates some sort of change in the background ionizing flux. Since this would produce the entire observed change in the b values, neither the He II Gunn-Peterson effect nor the expansion of pressure-confined models need be invoked.

Given the other problems with the pressure-confinement model outlined by Williger & Babul (1992), we must then ask whether it is plausible to have clouds which are *not* pressure confined by the IGM. The clouds might instead be gravitationally confined. For example, the CDM minihalo models of Murakami & Ikeuchi (1993) expand more slowly than the local sound speed and therefore have roughly thermal line widths with Doppler parameters in the $b = 15$–20 km s^{-1} range for the UV background fluxes found here. Depending on the exact details, these line widths could evolve in response to changing background flux, or they could increase as the minihalos are virialized at redshifts less than $z \sim 4$.

Another possibility is that the clouds are not confined by anything and that at $z = 4.3$ we are seeing a short-lived population which is either freely expanding or collapsing to form present-day galaxy halos. Expansion-cooled clouds have been shown to produce low values of b (Duncan, Vishniac, & Ostriker 1991). Williger (1991) found that the Doppler parameter would be ~ 20 km s^{-1} for models of freely expanding systems (at $z = 3.5$) and that these would evaporate on ~ 200 Myr timescales. By $z \sim 2.5$, these systems would have disappared and we would observe a quasi–gravitationally bound population with higher Doppler parameters. The steeper redshift dependence of the number of systems at the highest redshifts provides some support for this picture.

Collapsing galaxy halos, on the other hand, would disappear from view because of their decreasing cross section. Such a mechanism could also explain the anomalous line distribution described in § 4.1, since some degree of proto-galaxy clustering would be consistent with the clustering of present-day galaxies.

The ionization parameter found above, under the assumption that the lines have thermal widths, produces a neutral hydrogen fraction $n_{\rm H\,I}/n_{\rm H} = 9 \times 10^{-4}$. If the clouds are ionized by the background flux, the gas density at redshift $z = 4.3$ is $n_{\rm H\,I} = 2.5 \times 10^{-3}$ cm^{-3}. The thickness of a typical $N_{\rm H\,I} = 10^{14}$ cm^{-2} cloud is then only ~ 0.05 kpc. This should be compared to size estimates at least two orders of magnitude larger, from absorption systems in front of gravitationally lensed QSOs (Foltz et al. 1984; Smette et al. 1992). While all of the available statistics are consistent with viewing a population of very lightly flattened clouds with random orientations (see Milgrom 1988), this conclusion will not hold if the line widths are not thermal, if the ionizing flux is not that deduced from the proximity effect, or if the clouds are not in thermal equilibrium. The latter is relevant because the timescale to reach thermal equilibrium exceeds the available time before $z = 4.3$ for densities below $n_{\rm H\,I} = 10^{-3}$ cm^{-3}, close to the values discussed here.

6. CONCLUSIONS

We have fitted Voigt profiles to a 12 km s^{-1} resolution spectrum of the $z = 4.5$ QSO BR 1033−0327 and have found the following in the Lyα absorption lines with neutral hydrogen column densities in the range $13.3 \leq \log N_{\rm H\,I} \leq 18.0$:

1. The $(1 + z)$ power-law index γ for the redshift density of the Lyα systems depends on the H I cutoff chosen and is subject to losses in blends at high redshifts. This leads to an underestimate of the index. For systems with $\log N_{\rm H\,I} > 14.5$ cm^{-2}, line-blending effects should be small, and for these we find that $\gamma = 4.6 \pm 0.7$ gives a good fit over the redshift range $1.86 < z < 4.3$. However, at lower redshifts and lower column density limits, the power-law index appears to be lower. This may indicate that γ depends on the H I column density, but it is also consistent with the idea that the number density of systems for $3.7 < z < 4.3$ has a stronger redshift dependence than that found for $1.86 < z < 3.27$.
2. After an approximate correction for blending, the H I column density distribution is consistent with that at lower redshifts.
3. The ionizing background flux at $z \sim 4.2$ deduced from the Lyα blanketing of the continuum is $J_\nu \sim 1$–3×10^{-22} ergs cm^{-2} s^{-1} Hz^{-1} sr^{-1}. This is smaller by 0.5–1 dex than the value found at $z \sim 2.5$.
4. The characteristic Doppler parameters at $z \gtrsim 4$ are ~ 4 km s^{-1} lower than at later epochs.
5. The smaller Doppler parameters are consistent with the lower values of ionizing background flux inferred from the proximity effect. This suggests that the lines with b near the peak value do indeed have thermal widths, which in turn implies that the clouds are not pressure confined. The clouds could instead be gravitationally confined, or their numbers may be dominated at $z \sim 4.3$ by a population of short-lived clouds which have dissipated or collapsed by $z \lesssim 3.5$.

We are grateful to the CTIO staff for assistance at the telescope, John Webb for development of the profile-fitting software, Michael Rauch for the computer program to examine the two-point correlation function, Gary Ferland for his photoionization code, Avery Meiksin, Jordi Miralda-Escudé, Martin Rees, and Bob Williams for useful conversations, and a referee for very helpful detailed comments on the manuscript.

REFERENCES

Bajtlik, S., Duncan, R. C., & Ostriker, J. P. 1988, ApJ, 327, 570
Baron, E., Carswell, R. F., Hogan, C. J., & Weymann, R. J. 1989, ApJ, 337, 609
Bechtold, J. 1987, in High Redshift and Primeval Galaxies, ed. J. Bergeron, D. Kunth, B. Rocca-Volmerange, & J. Tran Thanh Van (Gif sur Yvette: Editions Frontières), 397
———. 1994, ApJS, 91, 1
Bond, J. R., Szalay, A. S., & Silk, J. 1988, ApJ, 324, 627
Carswell, R. F., Lanzetta, K. M., Parnell, H. C., & Webb, J. K. 1991a, ApJ, 371, 36
Carswell, R. F., et al. 1991b, ApJ, 381, L5
Carswell, R. F., Webb, J. K., Baldwin, J. A., & Atwood, B. 1987, ApJ, 319, 709
Chaffee, F. H., Jr., Foltz, C. B., Bechtold, J., & Weymann, R. J. 1986, ApJ, 301, 116
Duncan, R. C., Vishniac, E. T., & Ostriker, J. P. 1991, ApJ, 345, 39
Espey, B. R., Carswell, R. F., Bailey, J. A., Smith, M. G., & Ward, M. J. 1989, ApJ, 342, 666
Ferland, G. 1993, HAZY: An Introduction to CLOUDY, Dept. of Physics & Astronomy Internal Rep., Univ. Kentucky
Foltz, C. B., Weymann, R. J., Röser, H.-J., & Chaffee, F. H. 1984, ApJ, 281, L1
Ikeuchi, S., & Ostriker, J. P. 1986, ApJ, 301, 522
Irwin, M., McMahon, R. G., & Hazard, C. 1991, in The Space Distribution of Quasars, ed. D. Crampton (ASP Conf. Ser., 21), 117
———. 1994, in preparation
Jenkins, E. B., & Ostriker, J. P. 1991, ApJ, 376, 33
Lu, L., Wolfe, A. M., & Turnshek, D. A. 1991, ApJ, 367, 19
Madau, P. 1992, ApJ, 389, L1
Milgrom, M. 1988, A&A, 202, L9
Miralda-Escudé, J., & Ostriker, J. P. 1990, ApJ, 350, 1

Miralda-Escudé, J., & Rees, M. J. 1993, MNRAS, 260, 617
———. 1994, MNRAS, in press
Morris, S. L., Weymann, R. J., Savage, B. L., & Gilliland, R. 1991, ApJ, 377, L21
Murakami, I., & Ikeuchi, S. 1993, ApJ, 409, 42
Oke, J. B., & Korycansky, D. G. 1982, ApJ, 255, 11
Parnell, H. C. 1989, Ph.D. thesis, Cambridge Univ.
Pettini, M., Hunstead, R. M., Smith, L., & Mar, D. P. 1990, MNRAS, 246, 545
Press, W. H., & Rybicki, G. B. 1993, ApJ, 418, 585
Press, W. H., Rybicki, G. B., & Schneider, D. P. 1993, ApJ, 414, 64
Rauch, M., Carswell, R. F., Chaffee, F. H., Foltz, C. B., Webb, J. K., Weymann, R. J., Bechtold, J., & Green, R. F. 1992, ApJ, 390, 387
Rauch, M., Carswell, R. F., Webb, J. K., & Weymann, R. J. 1993, MNRAS, 260, 589
Sargent, W. L. W., Young, P. J., Boksenberg, A., & Tytler, D. 1980, ApJS, 42, 41
Smette, A., Surdej, J., Shaver, P. A., Foltz, C. B., Chaffee, F. H., Weymann, R. J., Williams, R. E., & Magain, P. 1992, ApJ, 389, 39
Storrie-Lombardi, L. J., McMahon, R. G., Irwin, M. J., & Hazard, C. 1994, ApJ, submitted
Williger, G. M. 1991, Ph.D. thesis, Cambridge Univ.
Williger, G. M., & Babul, A. 1992, ApJ, 399, 385
Wolfe, A. M. 1991, in Proc. ESO Mini-Workshop on Quasar Absorption Lines, ed. P. A. Shaver, E. J. Wampler, & A. M. Wolfe (ESO Sci. Rep. 9) (Munich: ESO), 97
Zuo, L., & Lu, L. 1993, ApJ, 418, 601